

LIBRARIES
MICHIGAN STATE UNIVERSITY
EAST LANSING, MICH. 48824

This is to certify that the

dissertation entitled

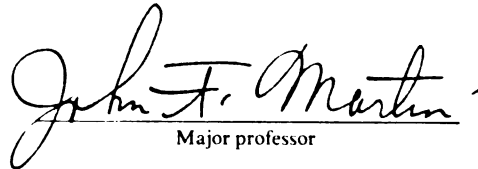
A Constitutive Modeling Technique Based on a Generalized
Rheological Model to Predict the Response of Materials

presented by

Barry L. Spletzer

has been accepted towards fulfillment
of the requirements for

Ph.D degree in Mechanics


Major professor

Date 2/24/84



RETURNING MATERIALS:
Place in book drop to
remove this checkout from
your record. FINES will
be charged if book is
returned after the date
stamped below.

--	--	--

**A CONSTITUTIVE MODELING TECHNIQUE BASED ON A GENERALIZED
RHEOLOGICAL MODEL TO PREDICT THE RESPONSE OF MATERIALS**

By

Barry L. Spletzer

A DISSERTATION

**Submitted to
Michigan State University
in partial fulfillment of the requirements
for the degree of**

DOCTOR OF PHILOSOPHY

Department of Metallurgy, Mechanics, and Materials Science

1984

ABSTRACT

A CONSTITUTIVE MODELING TECHNIQUE ON A GENERALIZED RHEOLOGICAL MODEL TO PREDICT THE RESPONSE OF MATERIALS

By

Barry L. Spletzer

A new constitutive modeling technique is developed that is capable of predicting typical uniaxial materials behavior at room and elevated temperatures. Simulation of the time-independent phenomena of cyclic hardening or softening, cyclic relaxation of mean stress and history dependent memory, and the time dependent behavior of creep and stress relaxation is accomplished. This constitutive model is based on generalized analysis of any configuration of classical rheological model elements and special purpose elements that were developed specifically for this constitutive modeling technique. For the analysis of notched members, a numerical technique is created to expand the Neuber relation model with the constitutive model to include time-dependent phenomena. A specific constitutive model was constructed from the material properties of Hastelloy-X. Three temperatures were considered, room temperature, 1200°F and 1600°F. Isothermal tests were performed on both smooth and notched specimens for the specific purpose of evaluating this constitutive model. A strain gage that is based on interferometric techniques is used to measure notch root strains at room temperature and 1200°F. This provided the unique opportunity to directly establish the validity and accuracy of the model for predicting inelastic time-dependent notch root strain response. In all cases the model predictions followed the general trend of the experimental data.

Correlation with the majority of the experimental data is very good. The most accurate predictions were at room temperature and the least accurate were at 1200°F.

To my father,
for the example and inspiration he
has provided throughout my life.

ACKNOWLEDGEMENTS

I would like to express appreciation to those who have helped and contributed to making this work a reality. This includes my advisor, Dr. John Martin, for his support, inspiration and assistance through this period; the National Aeronautics and Space Administration and Mike McGaw for their help in the experimental portion of the work; and the College of Engineering for its financial support. A final note of appreciation must go to my wife, Suzanne, and to my children, Ben and Katy, for their tolerance and encouragement.

TABLE OF CONTENTS

	Page
LIST OF FIGURES	vi
Chapter 1 INTRODUCTION	1
Chapter 2 GENERALIZED MODEL THEORY AND DEVELOPMENT.	5
2.1 Development of the Matrix Approach to Spring-Damper Modeling	5
2.2 Addition of Sliders to the Matrix Modeling Approach.	9
2.3 Addition of Special Purpose Elements to the Matrix Modeling Approach	14
2.4 Determining Model Response From a Strain Input	18
2.5 Incorporation of Neuber's Rule Into the Modeling Technique	19
Chapter 3 COMPUTATIONAL AND NUMERICAL CONSIDERATIONS OF THE GENERALIZED MODEL.	25
3.1 Overall Computational Considerations	25
3.2 Slider Analysis Considerations	27
3.3 Considerations of Neuber Simulation	31
Chapter 4 MODEL CONSTRUCTION TECHNIQUES	32
4.1 Overall Considerations	32
4.2 Element Configurations to Model Specific Behavior.	34
4.3 Basic Model Construction Examples.	35
4.4 Model Construction From Experimental Data.	40
4.5 Other Model Construction Techniques.	57
Chapter 5 DESCRIPTION OF EXPERIMENTAL EQUIPMENT AND PROCEDURES.	59

	Page
5.1 Test Equipment Description	59
5.2 Specimen Geometry.	60
5.3 Test Procedures.	62
Chapter 6 COMPARISON OF EXPERIMENTAL DATA WITH MODEL RESPONSE. .	65
6.1 Introduction	65
6.2 Comparisons at 1600°F.	65
6.3 Room Temperature Comparisons	68
6.4 Comparisons at 1200°F.	71
Chapter 7 CONCLUSIONS AND RECOMMENDATIONS.	77
LIST OF REFERENCES	80

LIST OF FIGURES

Figure		Page
1	Schematic Symbol and Response of an Elastic Spring . . .	8
2	Schematic Symbol and Response of a Viscous Damper . . .	8
3	Schematic Symbol and Response of a Frictional Slider. . .	11
4	Schematic Symbol and Response of a Cyclic Damper. . . .	17
5	Schematic Symbol and Response of an Irreversible Cyclic Element.	17
6	Illustration of Technique for Determination of Model Response at a Notch Root	22
7	Three Examples of Simple Spring-Slider Models Having the Same Response.	33
8	Spring-Slider Configuration Exhibiting Strain Level Triggering	36
9	Viscous Damper-Slider Configuration Exhibiting Strain Rate Triggering.	36
10	Cyclic Damper-Slider Configuration Exhibiting Strain Range Triggering	36
11	Stress-Strain Response of Cyclically Stable Hastelloy-X at 1600°F	41
12	Model Representation of Cyclically Stable Hastelloy-X at 1600°F	44
13	Comparison of 1600°F Hastelloy-X Model Response to Input Experimental Data.	46
14	Initial Response of Hastelloy-X at Room Temperature Subjected to Constant Strain Rate Testing	47
15	Model Representation of Room Temperature Hastelloy-X. . .	49
16	Initial Response of Room Temperature Hastelloy-X Model Subjected to Constant Strain Rate Testing	51

Figure		Page
17	Model Representation of 1200°F Hastelloy-X at Low Strain Rates	52
18	Comparison of Model and Experimental Response for Hastelloy-X at Low Strain Rates	54
19	Model Representation of 1200°F Hastelloy-X at Rapid Strain Rates.	55
20	Comparison of Model and Experimental Relaxation of Cyclic Mean Stress.	56
21	Smooth Axial Test Specimen Geometry	61
22	Hourglass Shape Diametral Specimen Geometry	61
23	Notched Specimen Geometry	63
24	Variable Strain Rate Input for 1600°F Test.	66
25	Comparison of Model and Experimental Response for 1600°F Test	67
26	Variable Strain Rate Input for Room Temperature Test.	69
27	Comparison of Model and Experimental Response for Room Temperature Test	70
28	Comparison of Model and Experimental Notch Root Response for Room Temperature Test.	72
29	Variable Strain Rate Input for 1200°F Test.	73
30	Comparison of Model and Experimental Response for 1200°F Test	74
31	Comparison of Model and Experimental Notch Root Response for 1200°F Test.	76

CHAPTER 1

INTRODUCTION

The development of the turbine engine for aircraft propulsion and of the reusable rocket engine has led to a demand for better understanding and prediction of the response of engineering materials which must operate at elevated temperatures. Accurate theoretical models to determine response under varying load either do not now exist, or else they are extremely complex so that they require extensive computational time for their use.

The prediction of stress-strain behavior near stress concentration sites is of utmost importance in evaluating the design of a part subject to severe service. The purpose of this work is to develop a simple and meaningful constitutive modeling technique which is capable of making such predictions by itself and, in combination with other techniques, such as the finite element method, may provide whole body results. Further, the modeling technique should use a minimum of experimental data to facilitate construction of the various material models which may be required.

The modeling technique chosen is a generalized approach to rheological modeling using frictional sliders and other special elements as needed. The use of frictional sliders in combination with classical rheological elements (elastic springs and viscous dampers) is not new. The combination of frictional sliders and elastic springs to model

material behavior was first suggested by Jenkins [1]* in 1922 and was published as textbook material by Timoshenko [2] in 1930.

Throughout the intervening years, the frictional slider has been used in the prediction of responses of materials and dynamic systems. In general, the materials response models have consisted of series combinations of matched parallel pairs of sliders and springs or parallel combinations of series pairs of sliders and springs [1, 3-7]. The dynamic models have been solely one or two degree-of-freedom models [8-12]. The technique developed here differs from these previous models in that it provides the capability for analysis of any general configuration of the available elements rather than only specific element configurations. This allows the required models to be developed from a wider range of experimental data since the type of model structure can be specifically tailored for ease of model parameter determination from the input experimental data.

Time dependent materials properties have been modeled by the incorporation of viscous dampers into the models [13, 14]. Again, such models have consisted of restricted and specific element connection geometries to model the specific phenomena which were observed. The technique developed here allows the incorporation of sliders with the springs and dampers in any configuration.

Certain material properties such as cyclic relaxation of mean stress and cyclic hardening or softening, which are not modeled implicitly by the spring and slider arrangements, have been modeled by making adjustments to the element parameters as required [15]. Two special

*Numbers in square brackets refer to the list of references. Numbers in parentheses refer to equations.

purpose elements are developed here to provide the capability of modeling these properties independently of the other element parameters. Again these elements may be used in any combination with the other types of elements.

The extension of the modeling technique to predict notch root responses requires the use of one relationship in addition to the constitutive model. The full response consists of three unknowns: notch or local stress, notch or local strain, and remote stress or strain with the remaining remote parameter being specified as the input. The constitutive modeling provides the relation that the material behavior is identical at both the local and remote locations. Any relationship between the local and remote response may be used and incorporated into the model to provide the desired results. Neuber's rule provides such a relationship as applied to monotonic response at a stress concentration [16]. The Neuber relation was chosen for its simplicity and the amount of experimental verification which has been conducted in its application to cyclic loading, by Bofferding [17], Lucas [18], Guillot [19], Leis and Topper [20, 21], and Topper, Wetzel, and Morrow [22] in this area. In the case of Bofferding, Lucas, and Guillot, the interferometric strain gage, developed by Sharpe [23, 24], was used to measure the notch root strains.

A technique is developed which incorporates Neuber's rule into the modeling technique. This provides for prediction of the notch root response of material subjected to complex loading at elevated and room temperatures.

Data for the construction of specific models are generated when needed, and the final results of the modeling are verified by conducting

various experiments using diametral and axial extensometers for nominal responses and the interferometric strain gage for notch root response.

CHAPTER 2

GENERALIZED MODEL THEORY AND DEVELOPMENT

2.1 Development of the Matrix Approach to Spring-Damper Modeling

The modeling technique employed provides for the use of elastic springs, viscous dampers, frictional sliders, cyclic dampers, and irreversible cyclic elements in any arrangement to simulate the stress-strain response of materials under complex loading. The theory supporting this technique is based on the ability to formulate matrix representations of the model parameters so as to provide a set of equations that may be solved numerically to determine the model response. The models will consist of the various types of elements with each element having two points where connection can be made to other elements, to a fixed reference frame, or to the point where the model response is measured. These connection points will be termed the nodes of the model. The model theory will be explained in sections beginning with the simplest model type, one composed entirely of elastic springs, and progressing to the complete general model representation and solution.

Any arrangement of linear springs may be modeled analytically by the relationship:

$$[E]\{s\} = \{\sigma\}^*$$
(1)

where $[E]$ is the stiffness matrix whose elements E_{ij} are determined by

*The equations presented use braces $\{\}$ to indicate column matrices, square brackets $[\]$ for square matrices and parentheses $()$ or no brackets to indicate scalar quantities.

computing the force at node i caused by a unit displacement at node j for a spring connected between nodes i and j . This is identical to the stiffness matrix formulation used in discrete vibrations [25] with the units converted from load and displacement to stress and strain. Each spring is connected to two node points and, in general, $[E]$ may be constructed from a zero matrix by adding the spring constant to the E_{ii} and E_{jj} elements and subtracting it from the E_{ij} and E_{ji} elements for a spring connected between nodes i and j . The $\{s\}$ matrix consists of the strains at the node points and $\{\sigma\}$ is the column of applied nodal stresses. When the stress input is known, which, for a one-dimensional model, is the input stress applied to only one node, the resulting nodal strains are readily calculated by:

$$\{s\} = [E]^{-1}\{\sigma\} \quad (2)$$

Generally, only the output strain of the single node where the stress is applied is considered to be the model response. The stress-strain response and schematic symbol of a single linear elastic spring are shown in Figure 1. The parameter E in the figure is the elastic stiffness of the spring expressed in units of pressure or stress (ksi or MPa).

Time-dependent creep may be incorporated into the model by the addition of viscous dampers. A damping matrix $[C]$ may be constructed in a manner analogous to that of the stiffness matrix $[E]$ resulting in:

$$[C]\{\dot{s}\} = \{\sigma\} \quad (3)$$

The matrix $\{\dot{s}\}$ is the derivative with respect to time of the nodal strains. The stress versus strain-rate response and schematic symbol of

a viscous damper are shown in Figure 2. The parameter C is the damping coefficient of the element expressed in units of ksi-seconds or MPa-seconds.

The two systems of equations may be directly combined to yield the total stress:

$$[C]\{\dot{\epsilon}\} + [E]\{\epsilon\} = \{\sigma\} \quad (4)$$

At this point, the system of equations is identical in form and construction to the governing equations for a discrete vibrational system with a zero mass matrix [25]. This family of differential equations may be solved directly if the inverse of [C] exists [26], however, since the model is usually not determinant in terms of the dampers alone, [C] is normally singular. The solution to Equation (4) will be found numerically using an iterative technique. This does not restrict the solution method since a numerical solution will be necessary when the general model is analyzed. If it is assumed that the second and higher derivatives of $\{\epsilon\}$ with respect to time are small compared with $\{\epsilon\}$ and $\{\dot{\epsilon}\}$ then the value of $\{\epsilon\}$ at a suitably small time step dT from the current time may be represented as a truncated Taylor's series:

$$\{\epsilon_{n+1}\} = \{\epsilon_n\} + dT\{\dot{\epsilon}_{n+1}\} \quad (5)$$

The term $\{\epsilon_{n+1}\}$ are the nodal strains at a time dT away. The column $\{\epsilon_n\}$ is the current strain and $\{\dot{\epsilon}_{n+1}\}$ is the derivative with respect to time of $\{\epsilon\}$ evaluated at a time dT away. A new strain-rate, $\{\dot{\epsilon}_{n+1}\}$, may be calculated by substituting the future strain-rate into Equation (4) as follows:

$$[C]\{\dot{\epsilon}_{n+1}\} + [E]\{\epsilon_{n+1}\} = \{\sigma_{n+1}\} \quad (6)$$

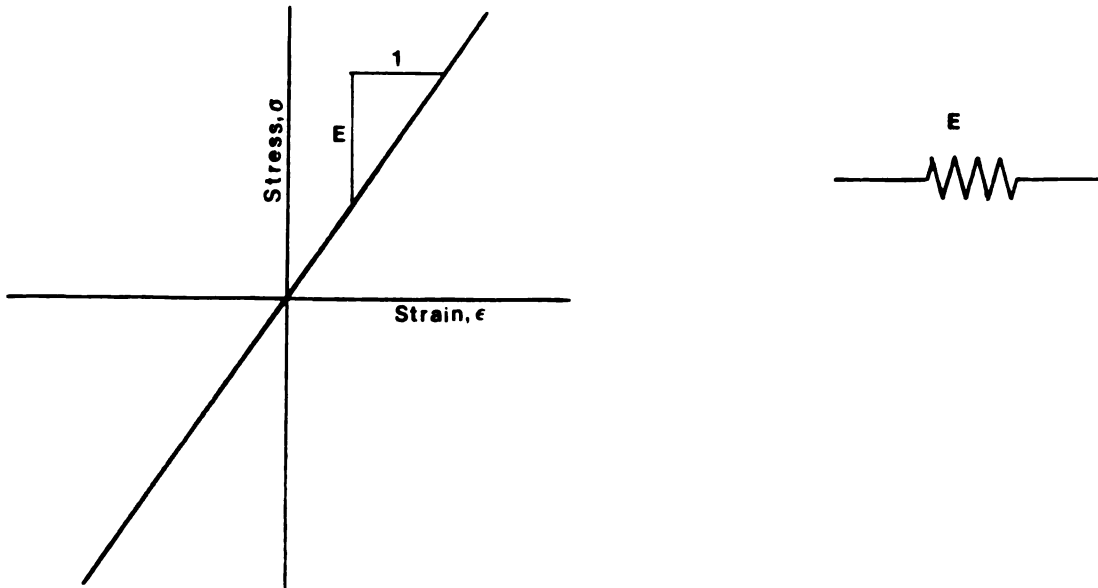


Figure 1: Schematic Symbol and Response of an Elastic Spring

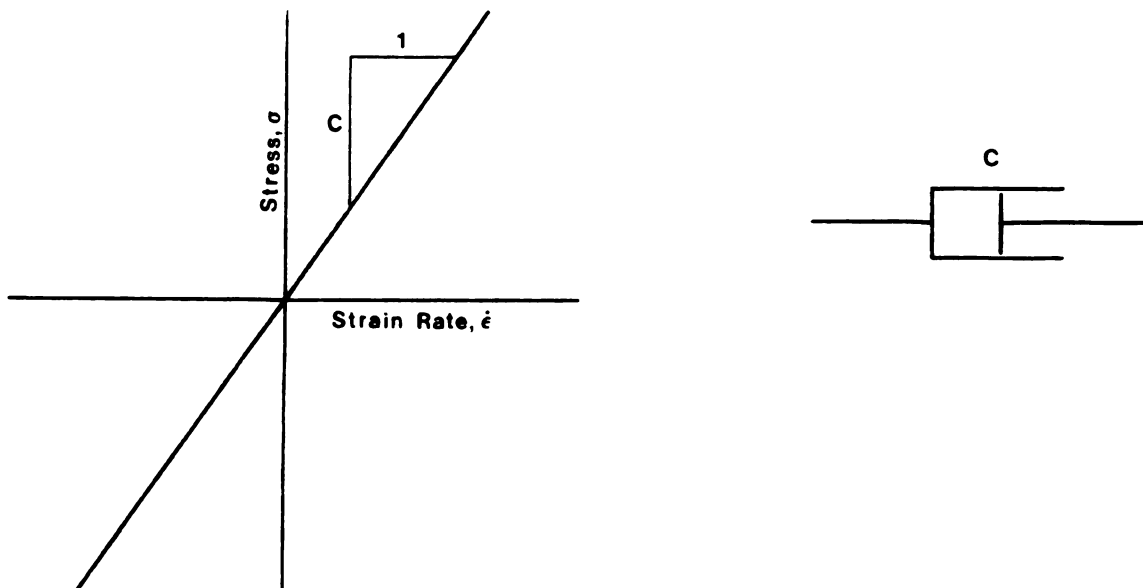


Figure 2: Schematic Symbol and Response of a Viscous Damper

Substituting the expression (5) into (6):

$$[C]\{\dot{\epsilon}_{n+1}\} + [E]\{\epsilon_n\} + dT\{\dot{\epsilon}_{n+1}\} = \{\sigma_{n+1}\} \quad (7)$$

rearranging terms:

$$[[C] + dT[E]]\{\dot{\epsilon}_{n+1}\} = \{\sigma_{n+1}\} - [E]\{\epsilon_n\} \quad (8)$$

Since the linear combination $[[C] + dT[E]]$ will generally not be singular for a model in which a connection exists from the fixed reference frame to the output node composed of only springs and viscous dampers:

$$\{\dot{\epsilon}_{n+1}\} = [[C] + dT[E]]^{-1}\{\{\sigma_{n+1}\} - [E]\{\epsilon_n\}\}. \quad (9)$$

Equation (9) gives the relation for the strain-rate at a time dT away in terms of the model parameters $[C]$ and $[E]$ and the known variables $\{\epsilon_n\}$, $\{\sigma_{n+1}\}$ and dT . The combination of Equation (5) with (9) allows for computation of the strain values at the end of the next time step as follows:

$$\{\epsilon_{n+1}\} = \{\epsilon_n\} + dT\{[[C] + dT[E]]^{-1}\{\{\sigma_{n+1}\} - [E]\{\epsilon_n\}\}\} \quad (10)$$

This completed solution will determine the stress-strain-time response of any collection of springs and dampers subjected to a known stress.

2.2 Addition of Sliders to the Matrix Modeling Approach

Engineering materials exhibit more complex behavior than can be modeled by a collection of linear springs and viscous dampers. Specifically, the elastic constant of most materials decreases with increasing stress and a memory effect is observed which gives rise to

stress-strain hysteresis loops. This behavior can be successfully modeled by the use of frictional sliders [1, 3-15] which are rigid within a specified stress range and provide opposing forces at the connecting nodes equal to the threshold stress if the loading is increased beyond the threshold value. Sliders which provide identical response in tension or compression will create the doubling or Masing effect [27] observed in many materials. Nonsymmetric sliders may be used to provide a tensile response which differs from the compressive response. Figure 3 shows the schematic representation and response of a typical slider in terms of a stress versus strain plot. The value S is the nominal threshold stress required to cause the slider to move. The distance between the upper and lower stress bounds of a slider is always $2S$ regardless of the degree of asymmetry selected. The parameter A determines the fraction of asymmetry of the slider and is the fraction of S by which the entire plot is shifted vertically. The dashed line in the figure indicates the response of the slider if the load is released after a strain value of ϵ_1 is reached. This shifting of the slider strain present at zero stress provides the capability to model the memory effects and hysteresis loops normally encountered in materials. Since the strain in a slider is indeterminate once the loading exceeds the threshold value, the sliders must be connected in parallel with determinant types of elements to yield a finite response to an input stress above the slider threshold. The initial rigid response (infinite elastic modulus) which would result if a direct connection between the fixed reference point and the output node consisted of sliders alone indicates that a real material will not contain such a connection.

In practice, the sliders are modeled by replacing all non-moving

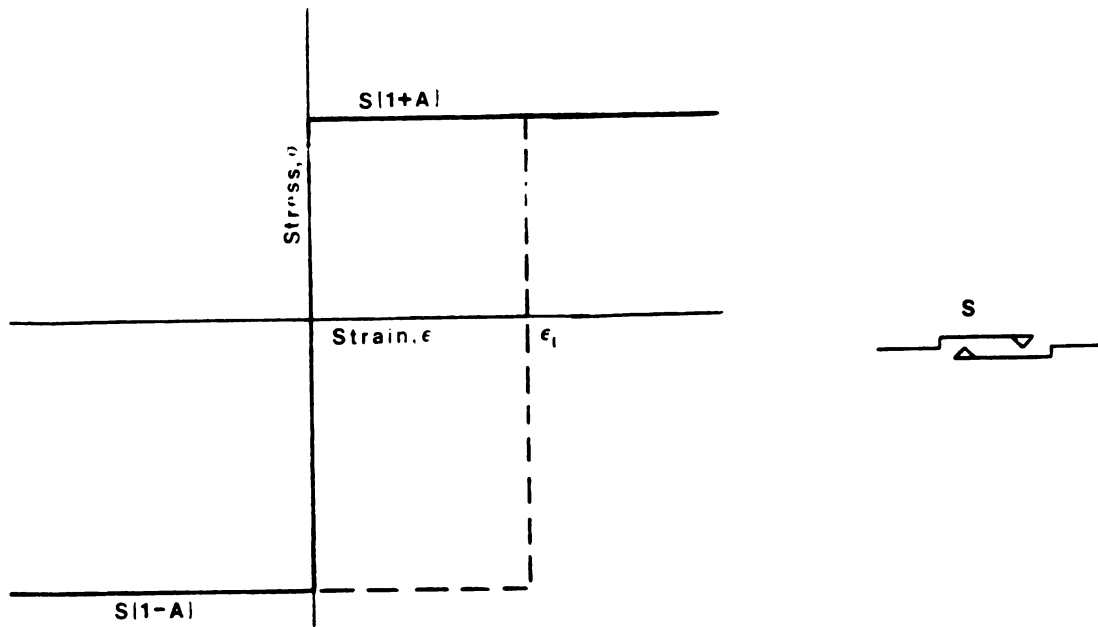


Figure 3: Schematic Symbol and Response of a Frictional Slider

sliders by very strong springs. The strain in these springs is then used to monitor the applied load to each of the sliders. When the load exceeds the specified threshold value, the spring is removed from the model and a stress equal to the threshold stress is applied to the nodes where the slider is connected. The forces are opposite and of a sign compatible with the state of the slider (tension or compression) at the time the threshold was reached. The opposing forces remain in effect until the relative strain-rate between the two nodes is reversed, at which time the springs are again installed in a fully extended or compressed position with the direction of the deflection dependent on the relative strain-rate between the end nodes of the slider. The replacement of the springs in the deflected position creates the hysteresis loop which is exactly double the monotonic stress-strain curve for symmetric sliders.

The incorporation of sliders into the matrix representation of the model will be explained using a slider stiffness matrix $[S]$, composed of the stiffness parameters of the strong springs which represent the non-moving sliders. The $[S]$ matrix is similar to $[E]$ in construction and characteristics, and it adds directly to $[E]$ to form the total elastic stiffness. The column matrix $\{F\}$ will represent the applied opposing nodal stresses which are used to simulate moving sliders.

The governing equation for the model can then be written by modifying Equation (4) as follows:

$$[C]\{\dot{\epsilon}\} + [[E]+[S]]\{\epsilon\} = \{\sigma\} + \{F\} \quad (11)$$

The major difference between $[S]$ and $\{F\}$ and the other model parameters, $[E]$ and $[C]$, is that $[S]$ and $\{F\}$ do not remain constant throughout

analysis of the model response. In particular, both [S] and {F} must be altered whenever a slider begins or stops moving (changes status).

Since the springs in [S] are released and reapplied at different strain values, the slider springs do not inherently possess a zero stress state which corresponds to zero strain. Therefore the product of [S] and {ε} in Equation (11) is not a true measure of the stress on a slider. The strain at which zero stress occurs must be computed and used to determine the actual stress in the slider springs. The zero stress values are in terms of relative strains or actual distance between the nodes common to each individual slider such that a single column of the nodal strains indicating the zero stress positions does not exist. However, for the purpose of this explanation, the column matrix {z} of zero stress positions will be used. A detailed explanation of how the zero stress positions are actually determined and used is included in the explanation of the computational considerations in Chapter 3. Equation (11) can be modified then by the inclusion of the {z} column to yield:

$$[C]\{\dot{\epsilon}\} + [E]\{\epsilon\} + [S]\{\{\epsilon\} - \{z\}\} = \{\sigma\} + \{F\} \quad (12)$$

This result may be applied directly to Equation (10) to yield the general relationship for determination of stress-strain-time response of any arbitrary combination of springs, sliders, and dampers. The zero stress position is of no concern when the stiffness matrices are being applied to strain-rates since the strain-rates are independent of the actual strain values. The final equation then becomes:

$$\{\epsilon_{n+1}\} = \{\epsilon_n\} + dT[[C] + dT[[E] + [S]]]^{-1}\{\{\sigma_{n+1}\} + \{F\} - [E]\{\epsilon_n\} - [S]\{\{\epsilon_n\} - \{z\}\}\} \quad (13)$$

2.3 Addition of Special Purpose Elements to the Matrix Modeling Approach

The above result is capable of modeling a wide range of materials behavior for a material which provides the same response under repeated identical cycles of loading (is cyclically stable). Actual materials frequently exhibit properties that vary with the number of loading cycles in a manner similar to that observed in time-dependent creep where the strain is a function of time as well as of stress. Equation (3) states the relationship between strain-rate and stress for viscous damping. An element analogous to the viscous damper is developed here which will provide reversible cyclic dependent properties. This element is termed a cyclic damper and behaves according to load reversals in a manner identical to the behavior of a viscous damper with respect to time. The viscous damper provides a resisting stress that is proportional to the applied strain-rate or the strain per time input. The cyclic damper provides a resisting stress that is proportional to the strain per reversal of loading. The behavior and schematic representation of such an element is illustrated in Figure 4 where the abscissa of the figure is in terms of strain per reversal of loading rather than strain per time as with viscous damping. The schematic symbol of the element is chosen to illustrate the ratcheting action which it can provide. The parameter D is the cyclic damping coefficient expressed in terms of stress multiplied by reversals. A collection of these elements would be governed by a relationship analogous to that of Equation (3) resulting in:

$$[D]\{d\epsilon/dR\} = \{\sigma\} \quad (14)$$

where $[D]$ is a cyclic damping matrix constructed from a set of cyclic

damping coefficients and node point connections similar to [E], [C], and [S]. The column $\{ds/dR\}$ is the derivative of node point strains with respect to reversals (half-cycles of loading). The Equation (14) must be expressed in terms of $\{\dot{\epsilon}\}$ to be of use in the model. This may be accomplished by noting that:

$$\{ds/dt\}(dt/dR) = \{ds/dR\} \quad (15)$$

For any specified loading, the time required for a reversal is known with this time being a constant equal to dt/dR which will be termed TT . Then Equation (14) becomes:

$$TT[D]\{\dot{\epsilon}\} = \{\sigma\} \quad (16)$$

The cyclic damping matrix can then be combined directly with the viscous damping matrix simply by replacing [C] with $[[C] + TT[D]]$ wherever it occurs. The incorporation of this fourth type of element, the cyclic damper, allows for general modeling of cyclic dependent behavior. The response of the cyclic damper is similar to the viscous damper in that both are completely reversible. The cyclic damping behavior is independent of the total number of reversals in the same way that a viscous damper responds independently of the total time elapsed. This element can, through use of suitable combinations, provide for a wide range of cyclically dependent reversible properties, such as cyclic relaxation of mean stress.

Properties which change irreversibly with cycling are frequently encountered and require the addition of another type of element to be properly modeled. Cyclic hardening and softening are examples of irreversible cyclic dependent properties. The element used to provide this

behavior is termed an irreversible cyclic element. These elements are connected between nodes like all other elements but do not possess a simple stress-strain response. The elements operate by assuming a certain fraction of the incremental stress which is applied to the entire model. This fraction varies irreversibly with continued cycling either up to a specified limit or from the limit to zero. This amount of stress is added in an equal and opposite manner to the two nodes to which the element is connected. Operating in this way, the element can cyclically harden or soften a material. When the irreversible elements are used in conjunction with viscous dampers, they will cyclically alter the time-dependent portion of the materials response. By allowing the irreversible element to reach an incremental stress-fraction-limit of one, the number of internal degrees of freedom of the model may be altered cyclically. The schematic representation and a plot illustrating the behavior of an irreversible cyclic element are given in Figure 5. The maximum strength coefficient, I , is the maximum fraction of the total applied stress increment which is to be applied at the element nodes and is unitless. Cyclic hardening may be modeled by the incorporation of these elements with an initial coefficient of zero and a final fraction or maximum strength coefficient between zero and one. Cyclic softening is modeled by varying the coefficient from a positive value to zero. The rate coefficient, R , determines the amount of variation which occurs per cycle of loading. The specified rate is approximately the number of element half-lives per reversal. A negative rate coefficient is interpreted as the element cyclically softening. The change in the strength coefficient per cycle is proportional to the specified rate and the amount of variation remaining in the element. This rate of change

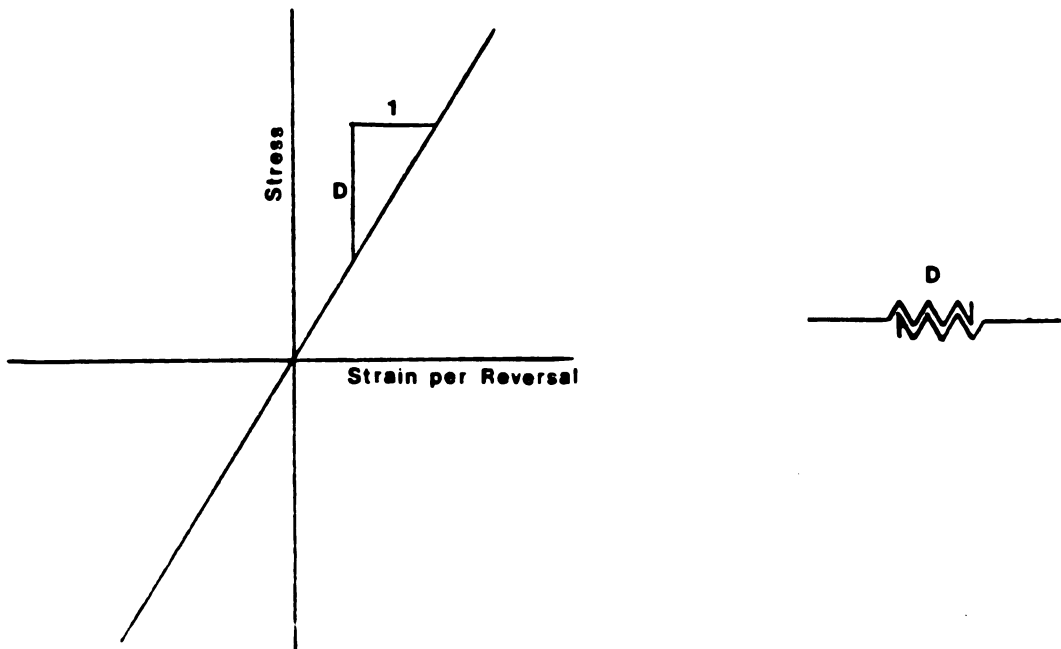


Figure 4: Schematic Symbol and Response of a Cyclic Damper

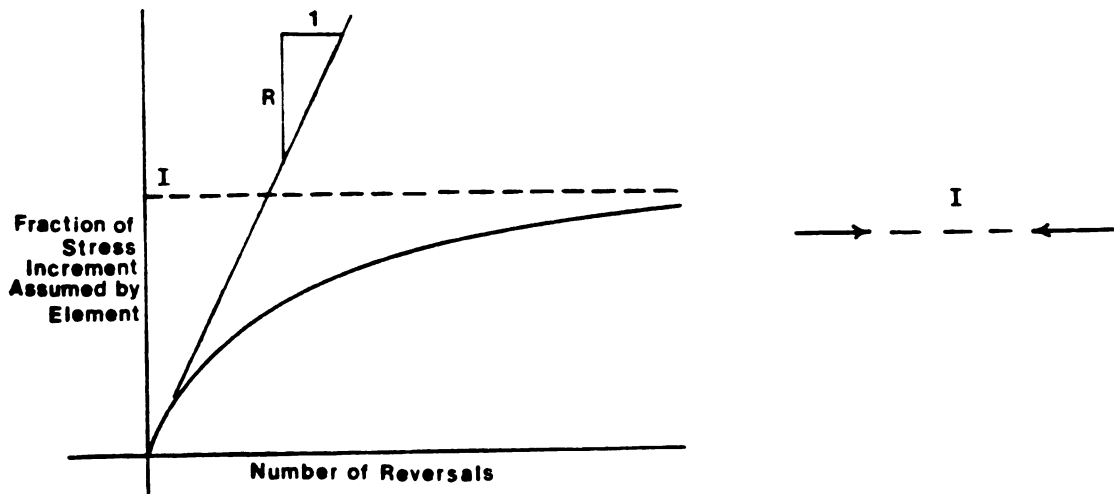


Figure 5: Schematic Symbol and Response of an Irreversible Cyclic Element

determination method provides for cyclic variation in an exponentially decaying fashion which is in good agreement with typical experimental data.

The irreversible elements are treated such that the strength coefficient changes only when there is motion between the two endpoints of the elements. In this way, irreversible elements in parallel with sliders will only change properties while the sliders are active. This allows for the modeling of strain-range-dependent cyclic hardening and softening.

2.4 Determining Model Response From a Strain Input

The above model formulation requires the input of known changes in stress for the time step chosen. Frequently, the stress response of a material under controlled strain conditions is desired. In such cases, the input will be in the form of known strain values and rates of the output node (m) for known time steps. The governing equation used to determine nodal strains (13) must be restructured to provide a solution in terms of the internal node strains and the stress at the mth node in terms of the known mth node strain. Equation (8) may be rewritten in the form:

$$[K]\{\dot{\epsilon}_{n+1}\} = \{\sigma_n\} - [E]\{\epsilon_n\} \quad (17)$$

Where now the unknowns are the first m-1 elements of $\{\dot{\epsilon}_{n+1}\}$ and the mth and only non-zero term of $\{\sigma_n\}$ which represents the total applied stress. The matrix $[K]$ is the linear combination $[[C]+dT[E]]$. The mth column of the $[K]$ matrix multiplied by the mth element of the $\{\dot{\epsilon}_{n+1}\}$ column may be transferred to the right side of the equation. This

column is then replaced in the $[K]$ matrix by a column of zeroes with a -1 in the m th position which represents the $\{\sigma_n\}$ column moved to the left side of the equation. This results in an equation of the form:

$$[K^*]\{\dot{\epsilon}_{n+1}^*\} = -\{epc\} - [E]\{\epsilon_n\} \quad (18)$$

Where the starred matrices have been modified as indicated and the column $\{epc\}$ is that constructed from the m th node strain-stiffness product as explained. Now the first $m-1$ elements of the $\{\dot{\epsilon}_{n+1}^*\}$ column are the nodal strain-rates of the internal nodes and the m th element is the required applied stress to meet the imposed applied strain constraints. This technique may be extended directly to the complete model containing all element types with no alteration. After solving the system of equations in a manner identical to that explained before, the strain-rate and stress columns are rearranged to the normal state to allow the remainder of the model response solution to proceed in the same manner for either stress or strain control. This allows the solution of the irreversible cyclic elements to be completely unaffected by the type of model inputs.

2.5 Incorporation of Neuber's Rule Into the Modeling Technique

The general rheological modeling approach allows the stress-strain behavior of a material to be predicted provided that either the stress or strain level is known as a function of time. Frequently, the nominal stress or strain of a part in service may be well known while the stresses and strains at a critical location are desired but not known. The modeling technique may be used to provide the capabilities for prediction of local material response whenever some relationship between the

nominal and local responses is available.

Once such a relationship is determined, it may be combined with the model behavior at both the remote and local positions to provide three independent equations in terms of the four material response parameters: remote stress, remote strain, local stress and local strain. This allows the response of the material in terms of local and remote stresses and strains to be predicted from a single input consisting of the remote stress or strain input.

Neuber's rule provides a relationship between the nominal stress and strain and the stress and strain at a stress concentration. This relationship may be written for cyclic behavior as:

$$\Delta\sigma \cdot \Delta\epsilon = \Delta S \cdot \Delta E \cdot k_t^2 \quad (22)$$

where $\Delta\sigma$ is the change in stress at a critical location (notch root) since the last reversal of loading and $\Delta\epsilon$ is the change in notch root strain. ΔS and ΔE are the remote or nominal changes in stress and strain since the last reversal and k_t is the elastic stress concentration factor.

The general solution of the notch root stresses and strains then involves three unknowns (σ , ϵ , and E for example when S is known) to be solved when a single input is known. The notch root response may then be determined analytically once the model has been formulated and the nominal stress or strain along with the elastic stress concentration factor is known.

The analysis is performed by first applying the nominal stress or strain history to the model and determining the model response. This response is then used in conjunction with Neuber's rule to direct the

stress input at the critical location. The generalized modeling technique requires the stipulation of small time steps and the application of the corresponding change in stress to the model over the time step. The time steps used in the Neuber simulation are taken directly from the stress-strain-time data generated for the nominal response. The corresponding change in stress (either stress or strain may be used) is determined by extrapolating linearly the last portion of the local stress-strain response to its intersection with the closest sheet of the hyperbola which describes the Neuber relation at the end of the current time step being solved. The general derivation of this solution is explained below and illustrated in Figure 6.

If the local stress-strain response is known at two points corresponding to t_n and t_{n-1} and the change in local stress to reach time t_{n+1} is to be determined, the local stress-strain curve may be extrapolated linearly using the point slope solution of the line:

$$\sigma_{n+1} = (\sigma_n - \sigma_{n-1}) / (\epsilon_n - \epsilon_{n-1}) \cdot (\epsilon_{n+1} - \epsilon_n) + \sigma_n \quad (23)$$

where the various subscripts refer to the values of the parameters at the corresponding times. The hyperbola which defines the Neuber relation at time t_{n+1} is:

$$\Delta\sigma_{n+1}\Delta\epsilon_{n+1} = \Delta S_{n+1}\Delta E_{n+1}k_t^2 \quad (24)$$

Where the values ΔS_{n+1} and ΔE_{n+1} are determined from the nominal material response. A relationship between the delta parameters (i.e. ΔE) and the absolute parameters (i.e. E) is also needed to solve for the stress change. This relationship is, of course:

$$E = \Delta E + E_r \quad (25)$$

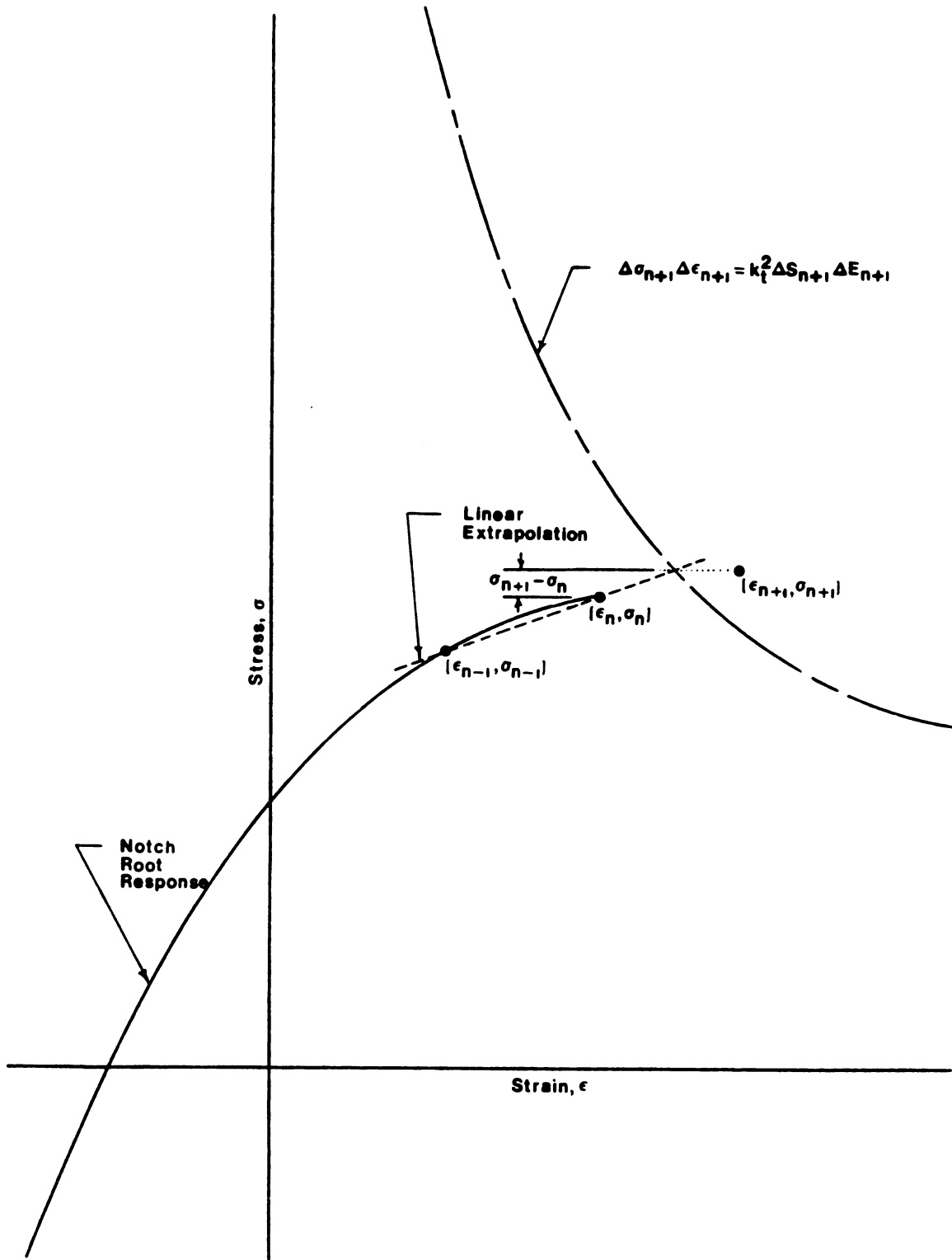


Figure 6: Illustration of Technique for Determination of Model Response at a Notch Root

Where the subscript r denotes the value of the parameter at the time of the last reversal or at the beginning of the modeling, whichever is more recent. Equations (23), (24), and (25) may be combined in such a way as to eliminate the ϵ_{n+1} terms yielding a quadratic in terms of $\sigma_{n+1}-\sigma_n$ which is the linearized estimate of the change in notch root stress to be used in the generalized model solution of the current time step. The two solutions for the quadratic represent the intersection of the straight line extension with both sheets of the hyperbola. Only the nearest intersection is of interest since the farther sheet lies on the far side of the stress-strain state at the beginning of the current reversal. The equation for the change in notch root stress is:

$$\sigma_{n+1}-\sigma_n = \text{SIGN}(B) \cdot (B^2 - M(\Delta\sigma_n \Delta\epsilon_n - k^3 \Delta S_{n+1} \Delta E_{n+1}))^{1/2} - B \quad (26)$$

where the $\text{SIGN}(B)$ term provides the solution of the nearest sheet and the values B and M are defined as:

$$B = (\Delta\sigma_n + M \Delta\epsilon_n) / 2 \quad (27)$$

$$M = (\sigma_n - \sigma_{n-1}) / (\epsilon_n - \epsilon_{n-1}) \quad (28)$$

This solution is depicted graphically in Figure 6 showing the extrapolation of the local stress-strain response to the intersection with the current Neuber relationship. Note that the errors induced by the linearization are highly exaggerated in Figure 6 and are, to some extent, self correcting since the next Neuber hyperbola is recalculated independently of the local response for each subsequent time step.

The change in notch root stress found by this technique and the time step taken from the nominal response are used as inputs for the general rheological model. The model uses this information to determine

the change in notch root strain during the time step which provides the needed values of local stress and strain to be used during solution of the subsequent time step. This method in this way satisfies the Neuber relation in a stepwise manner through linearized approximations of the stress changes. The amount of error inherent in this process depends on the departure from linearity of the local stress-strain curve. The steps must be chosen sufficiently small such that this departure has negligible effects on the overall results of the computations. This constraint is not limiting since the same considerations apply to the truncated Taylor series used in the development of the generalized rheological modeling technique.

CHAPTER 3

COMPUTATIONAL AND NUMERICAL CONSIDERATIONS OF THE GENERALIZED MODEL

3.1 Overall Computational Considerations

The theoretical development of the generalized model presented in Chapter 2 does not deal with the computational subtleties which are inherent with the implementation of this modeling technique. This chapter presents several considerations concerning implementation of the modeling technique into any computing system. These considerations will be presented in the same sequence as the corresponding portions of the model were discussed in Chapter 2.

The output stress matrix $\{\sigma\}$ consists of a column of zeroes, representing the zero applied stress at the internal nodes, with a single non-zero element representing the applied model stress at the output node. There is no necessity to maintain the entire $\{\sigma\}$ column, and only the current stress value is stored to be added to the remainder of the right hand side of the governing equation as needed.

The selection of a suitable time step (termed dT) requires a tradeoff in terms of computing time. The assumption surrounding the use of a sufficiently small time step or the justification of a two term truncated Taylor's series is that the second and higher derivatives of the strain with respect to time are small compared with the first derivative or, more directly, the curvature of the strain-time response is slight. The value of dT could be chosen on this criterion alone through use of a finite difference approximation of the second derivative such that the

largest acceptable value of time step would always be used to minimize the number of steps required to solve a given problem. However, the final governing equation (13) in Chapter 2 shows that the indicated matrix inversion need only be performed when the time step or $[S]$ is altered. Since the inversion process is by far the most time consuming portion of the computation, the selection of a uniform time step which is changed only when $[S]$ is altered will minimize computation time. The $[S]$ matrix is altered extensively at the end of each reversal and the time step for the next reversal is chosen at that time by dividing the total time of the next reversal into an integral number of parts. Experimentation with various numbers of time steps has shown a value of 50 steps per reversal to be adequate for all models tested. Some increase in computational speed may be desirable for the analysis of very large models; in which case the redetermination of the time step whenever a slider changes status should be considered.

The use of stress or strain control for conducting the modeling presents no special numerical problems. Difficulties do arise in the choosing of a time step for certain combinations of control conditions. Whenever the driving input for the model and the imposed limit are not of the same type (i.e. an input stress-rate with a maximum strain limit), the time required to complete the input is unknown and the time step cannot be directly determined. In such cases it would be possible to determine a time step based on the curvature of the strain-time response. This determination would assure that the linearization assumptions of Chapter 2 were not violated in areas of sharp strain-time response curvature. Further, it would allow the value of the time step to be increased when the degree of curvature became small. A new time

step would be calculated as seldom as possible to preserve some of the computing economy of the constant-time-step technique. Such a procedure has not been required to this point, but it could be developed.

3.2 Slider Analysis Considerations

The analysis of frictional sliders requires the use of several special techniques that are not apparent from the matrix representation of the sliders. The determination of the individual slider stiffnesses to be used may be done in any manner as long as the equivalent slider springs are stiff enough to appear rigid when compared to any elastic spring used. The use of the very stiff springs allows for analysis of redundant (statically indeterminant) slider arrangements which would be difficult to solve if rigid links were used. For simplicity in sensing the beginning of slider motion, slider stiffnesses are initially determined such that all sliders begin to move at the same value of individual slider strain. This requires sliders with higher threshold values to be proportionately more stiff than lower valued sliders. The slider stiffness is chosen with the weakest slider being 1000 times more stiff than the strongest spring. This convention provides for a maximum error induced by the nonrigid sliders of no more than 0.1% of the total response.

The non-analytic nature of the frictional slider, particularly the lack of a constant zero, coupled with the high stiffness provides some numerical difficulties in determining the actual slider strains which are needed to determine the slider status. Typically, the absolute strain at a given node point will be 3 to 5 orders of magnitude larger than the relative strain on a given slider. The relative slider strain

is determined by the difference in the absolute strains at the endpoints of the slider. This computation of slider strain by subtraction of values which are very close together requires that at least 10 significant digits be maintained in both the absolute nodal strain values and the strain-rate values.

The majority of model parameters are constant throughout the analysis of the model response. Specifically, the matrices $[E]$, $[C]$, and $[D]$ are constant as are the node point connections of the individual sliders. These matrices are maintained as would be expected. The slider stiffness matrix $[S]$ is not constant and must be altered whenever a slider starts or stops moving. The $[S]$ matrix could be maintained as the other model matrices with repetitive additions and subtractions being performed to adjust the matrix as needed. Such operations would result in eventual round-off error, especially since the elements in $[S]$ are several orders of magnitude greater than the elements of $[E]$ and $[S]$ is always added to $[E]$ when it is to be used. This problem is avoided by maintaining $[S]$ only in terms of the individual slider stiffnesses, node point connections, and slider status (moving or stopped). The appropriate values are then added directly to the elements of $[E]$ when $[E+S]$ is needed in the analysis. The large difference in magnitudes of the elements of the combined $[E]$ and $[S]$ matrices requires that at least 10 significant digits be carried during the inversion process.

The nature of the frictional sliders causes the overall stiffness of the model to be discontinuous at any point when a slider changes status. The possibility of one or more sliders changing status during a single time step prohibits the use of the linearization assumption upon which the entire model solution is based. Sliders cannot be restricted

to change status only at the end of a time step but must be allowed to change whenever the threshold stress is reached. This difficulty is overcome by using a temporary time step which is adjusted back to the time when a slider threshold is reached. At the end of each time step, the relative strain on each slider is compared with the maximum allowable strain. The slider which exceeds maximum allowable strain by the greatest fraction of incremental strain during the time step is chosen as the single slider which will begin to move. The time step, applied stress, all nodal strains, and irreversible cyclic forces are then linearly relaxed to the point when that threshold value was reached. The solution then proceeds as usual. If several other sliders also exceed the maximum allowable strain during a given time step, this linear relaxation procedure will reduce all such slider strains to an allowable value. The several other sliders will be treated in subsequent temporary time steps merely by returning the solution technique to the normal mode and determining the next slider to release in sequence. The use of the temporary time step and linear relaxation of the model parameters does not require a separate analysis of the model response at the altered time step which precludes the need for an additional matrix inversion as each slider begins to move. An inversion is required following the change in slider status, however.

The transition of sliders from a moving to a stopped state cannot be done in a sequential manner as when sliders begin moving. Generally, a reversal of loading will stop all moving sliders simultaneously. This produces a very large discontinuity in the model stiffness which is difficult to accurately predict. The use of time-dependent elements in the model provides the possibility that some sliders will not stop at a

reversal, requiring a technique be developed to monitor the status of each slider after the reversal. The action of a slider stopping is sensed by a reversal in the relative strain direction of the connecting nodes. Such a reversal indicates that the force in the {F} array must be removed and the stiffness coefficients in [S] be replaced. The sliders which stop are sensed by using a very small time step (.01 of the standard step) immediately following any reversal of loading. The response of the model is analyzed for the small step after which the status of all appropriate sliders is altered. The amount of error introduced by the small time step is very small compared with the overall model response (about 0.02%) and is eliminated to a great degree by automatically deleting the data point determined this way. Once the necessary sliders are altered, the solution proceeds in the usual manner.

When a moving slider stops, the threshold values of slider strain must be updated. All sliders have the same allowable strain-range in which they are considered stationery, with the individual slider threshold stress being attained at the endpoints of this range. Initially, all symmetric sliders are in the middle of the range. Whenever a reversal occurs, the moving sliders are at one end of the range and the elastic slider strain for those which stop is updated to indicate this. This provides the doubling phenomenon which is observed in many materials and which is modeled naturally by the frictional slider. Asymmetric behavior is introduced by altering the zero stress point within the elastic slider range such that it lies closer to one elastic strain limit than the other.

The modeling of the moving sliders consists of the treatment of the

applied internodal forces termed {F} in Chapter 2. This column is not maintained in strict column form, primarily because of accumulated round-off from repeated additions and subtractions, but it is maintained as an array with a width equal to the number of sliders in the model. This method allows {F} to consist entirely of zeroes and individual slider threshold values. The technique also simplifies construction and maintenance of the array.

3.3 Considerations of Neuber Simulation

The equations derived from the incremental solution of the Neuber relation do not deal with any of the various model matrices and therefore do not require extensive numerical considerations. The use of reduced time steps to sense the slider status following each reversal provides the possibility that both the future Neuber hyperbola and the linear extrapolation of the local response are greatly in error for a single data point pair. This difficulty is greatly reduced by not using the first point following a reversal as a valid data point. Small aberrations in the data may result in similar problems that are not as simply solved. Such aberrations may result in only complex solutions to Equation (26). Because of this, whenever a complex solution is encountered, the previous linear interpolation equation is used to predict the intersection point. This procedure introduces very little error into the overall response but allows the solution to continue as usual. If unacceptable results are still obtained, the nominal response data could be smoothed using numerical techniques which would assure that the individual data points follow the general trend of the surrounding points.

CHAPTER 4

MODEL CONSTRUCTION TECHNIQUES

4.1 Overall Considerations

The use of arbitrary configurations of simple, special purpose elements provides the capability to model many of the stress-strain phenomena observed in actual materials. This capability is of practical benefit only if techniques can be developed to convert basic experimental data into general models capable of predicting the response of a material when subjected to complex loadings. This chapter presents several specific techniques and general guidelines which may be used to construct such models and specific examples of model construction.

The determination of an adequate model to provide a certain response is not a unique process in that a number of different models may exist which will have the same response. An example of three simple spring and slider arrangements which all exhibit the same response is given in Figure 7. All models in this example consist of three springs and two sliders but in each case the values of the springs and sliders must be different to provide the same response. This example is not unusual since multiple models usually exist. The existence of multiple models can be visualized in terms of the governing matrix equations presented in Chapter 2. The model response has been defined as the stress and strain measured at a single output node. Models with identical response are only required to be identical in terms of the response

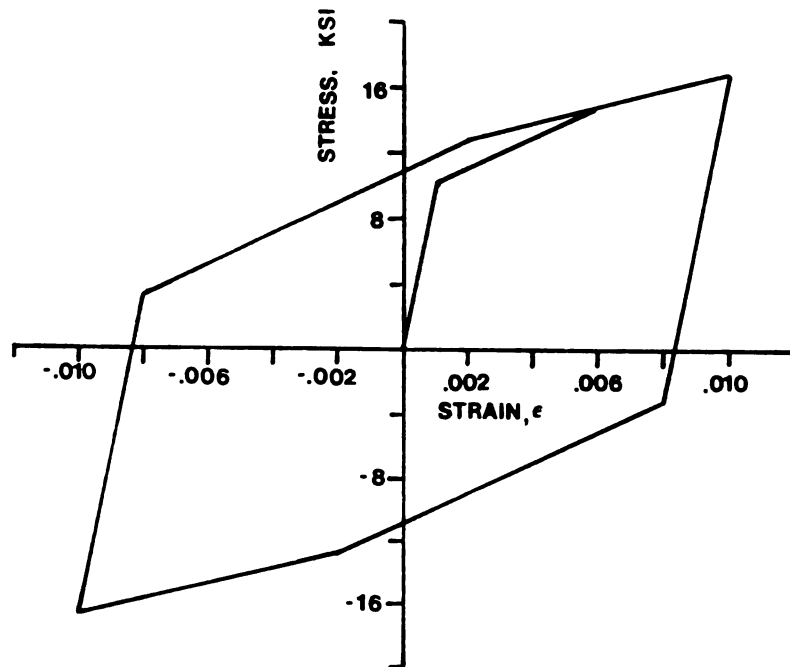
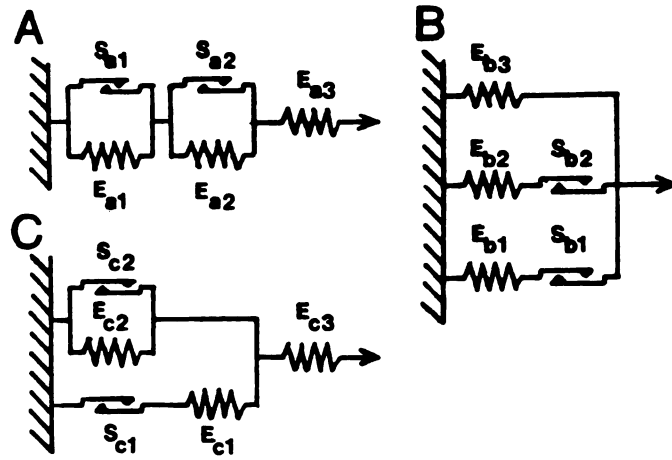


Figure 7: Three Examples of Simple Spring-Slider Models Having the Same Response

of that single node and it is conceivable that several different models could exist which provide identical response of that node. The internal nodes of the models will normally have different responses however. As more types of elements are added to the model, the ease of determining such models decreases rapidly. The large number of potential configurations available to model any particular response allows for a configuration determination technique to be tailored specifically to the available data since only a single adequate model is required.

4.2 Element Configurations to Model Specific Behavior

The use of frictional sliders in the modeling is necessary to provide material properties that change with the applied stress level and provide the familiar hysteresis loops. The slider, when placed in parallel with some collection of other elements, may be considered a stress trigger which will be released and allow the other elements in parallel with it to become active when the threshold stress is reached. There are other useful ways in which the slider may be combined to provide different types of triggering. Placing a slider in series with an elastic spring and using this combination in parallel with other elements provides what could be viewed as a strain trigger. Figure 8 illustrates such a configuration. When the strain on the spring (which is identical to the strain of the group of elements in parallel with the spring-slider combination) reaches S/E , the stress in the spring is the threshold value of the slider (S), and the slider begins to move providing a constant resisting force equal to S . Notice here that the spring slider combination does provide a linearly varying resisting force until the slider begins to move.

The slider may also be placed in series with a viscous damper to provide a strain-rate trigger as shown in Figure 9. This combination will cause the slider to release when the relative strain-rate between the end nodes exceeds S/C . Similarly, the slider may be combined with a cyclic damper, shown in Figure 10 to provide triggering only when the strain per reversal exceeds S/D . Such a configuration can provide properties which vary with strain range.

More complicated configurations of sliders with other elements could be used to provide a variety of responses.

4.3 Basic Model Construction Examples

The first examples of determination of model parameters will be for the three models (A, B, and C) in Figure 7 to provide the identical response shown. Each of the parameters for the three example models will be determined. These examples will illustrate the advantages of using both the strain trigger and stress trigger representation of slider-spring combinations.

The Model A configuration is a series arrangement which provides that the spring, E_{a1} , and the two parallel spring-slider combinations always experience a stress equal to the total applied stress. The slider thresholds are the breakpoints of the required stress-strain response which can be read directly from the initial stress-strain response shown in Figure 7. The slider values are then:

$$S_{a1} = 14.8 \text{ ksi} \quad S_{a2} = 10.0 \text{ ksi}$$

Initially, all sliders are fixed and the slope of the initial response is the elastic constant for E_{a1} , which may be determined from the

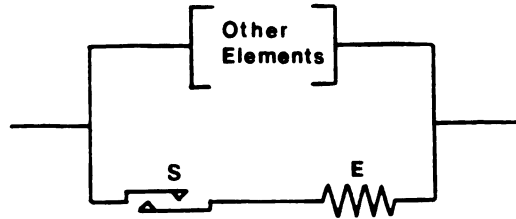


Figure 8: Spring-Slider Configuration Exhibiting Strain Level Triggering

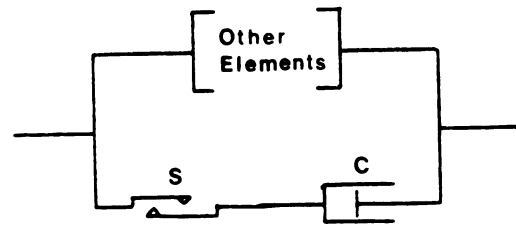


Figure 9: Viscous Damper-Slider Configuration Exhibiting Strain Rate Triggering

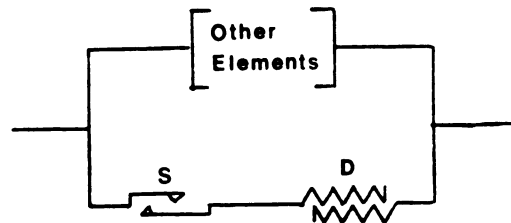


Figure 10: Cyclic Damper-Slider Configuration Exhibiting Strain Range Triggering

stress-strain value at the elastic limit, resulting in:

$$E_{a2} = 10.0 \text{ ksi} / .001 = 10000 \text{ ksi}$$

The value of E_{a2} may be calculated by noting that the required change in strain of .005 must occur over the stress change of 4.8 ksi. The 4.8 ksi increase in stress will cause an increase in strain of 0.00048 in E_{a2} , requiring the remainder of the strain occur in E_{a1} resulting in:

$$E_{a1} = 4.8 \text{ ksi} / (0.005 - 0.00048) = 1061.95 \text{ ksi}$$

The value of E_{a1} is determined in a similar way using a change in stress of 2.0 ksi over a strain change of 0.004. This results in:

$$E_{a1} = 2.0 \text{ ksi} / (0.004 - 0.0002 - 0.001883) = 1043.30 \text{ ksi}$$

This case uses the sliders as stress triggers and allows the slider threshold values to be determined immediately by inspection while the springs require some computation.

The model labeled B uses sliders in a configuration which allows the absolute value of strain to be of more interest since the three parallel segments of the model are all subjected to the same strain. The slope of the response above 14.8 ksi is the value of the spring E_{b2} , since at this point only E_{b2} continues to deform elastically. This value is:

$$E_{b2} = (16.8 - 14.8) \text{ ksi} / (0.010 - 0.006) = 500 \text{ ksi}$$

The slope between 10 and 14.8 ksi is achieved by the addition of E_{b1} and E_{b2} resulting in:

$$E_{b1} = 4.8 \text{ ksi} / 0.005 - 500 \text{ ksi} = 460 \text{ ksi}$$

The final spring is determined in a similar manner with the three springs adding to comprise the initial elastic response:

$$E_{b1} = 10 \text{ ksi} / .001 - 460 \text{ ksi} - 500 \text{ ksi} = 9040 \text{ ksi}$$

The sliders may be determined as a function of the strain at which they trigger. The slider S_{b1} releases at a strain of 0.001 which provides a stress on E_{b1} equal to the slider threshold value:

$$S_{b1} = 9040 \text{ ksi} * .001 = 9.04 \text{ ksi}$$

The slider S_{b2} releases at a strain of 0.006 resulting in:

$$S_{b2} = 460 \text{ ksi} * 0.006 = 2.76 \text{ ksi}$$

In construction of a model from strain controlled experimental data it would be reasonable to construct a parallel type model similar to the one illustrated to take advantage of the use of strain values rather than primarily stress values for triggering.

Model C is a combination of series and parallel modeling which is included to demonstrate that a model of another configuration may be constructed in a manner similar to that used for A and B. Here the initial response of the system is determined entirely by the spring E_{c1} so:

$$E_{c1} = 10000 \text{ ksi}$$

The remainder of the system is rigid until slider S_{c2} begins to move at 10 ksi. therefore:

$$S_{c2} = 10 \text{ ksi}$$

Once both sliders have been released, the spring E_{c2} must combine in

series with E_{c2} , to provide the final slope of 500 ksi. This results in:

$$\begin{aligned} E_{c2} &= (500 \text{ ksi} * 10000 \text{ ksi}) / (10000 \text{ ksi} - 500 \text{ ksi}) \\ &= 526.32 \text{ ksi} \end{aligned}$$

The effective stiffness of the parallel combination of E_{c2} and E_{c1} must combine with E_{c3} , to produce the slope of the response observed between 14.8 ksi and 16.8 ksi. This combination results in:

$$\begin{aligned} (16.8 \text{ ksi} - 14.8 \text{ ksi}) / (.006 - .001) &= (E_{c3} (E_{c2} + E_{c1})) / (E_{c3} + E_{c2} + E_{c1}) \\ E_{c1} &= 579.89 \text{ ksi} \end{aligned}$$

Finally, the slider S_{c1} may be determined from the strain value at its trigger point of .006 and the portion of the strain assumed by E_{c3} :

$$\begin{aligned} S_{c1} &= 579.89 \text{ ksi} * (0.006 - 14.8 \text{ ksi} / 10000 \text{ ksi}) \\ &= 2.621 \text{ ksi} \end{aligned}$$

While the models illustrated here do not involve the more complex elements available, the technique of working with the sliders is similar for any type of model, as will be apparent when more complex models are constructed.

The construction of models using viscous dampers together with elastic springs may be done by using the basic techniques of viscoelasticity to solve for the response of simple collections of these elements. In all cases where more complicated models are to be determined, access to an interactive computing system with graphic output is extremely useful to allow rapid comparison of proposed models with the available data to direct the final development of the specific model.

4.4 Model Construction From Experimental Data

The first model to illustrate the use of the viscous damper in modeling will be that of Hastelloy-X at a temperature of 1600°F. The data from which the model will be constructed consists of controlled strain-rate tests on a cyclically stable specimen at five different rates with the strain limits being ± 0.006 in all cases. The data, taken from Walker [28], are shown in Figure 11. The range of strain rates available covers three orders of magnitude which will illustrate the capability of the modeling technique to simulate a wide range of specimen response with a single model.

Construction of the model will begin by considering the slowest strain rate loop to be the result of a static tension test at 1600°F. This assumption is not overly limiting since the use of the model to predict the response of extended tests at strain rates lower than the available data is not reasonable. The strain rates for which predictions can be made should not exceed the limits of the data used to construct the model. This is also true of the stress and strain limits used. The modeling of the slowest strain rate can be done entirely with a series combination of spring-slider pairs similar to those used in the model A example previously. Subsequent alterations to the model to accommodate the change in response with increasing strain-rate will incorporate some degree of rate dependence into the slowest strain rate loop. The static model is determined by approximating the slowest strain rate loop by a series of straight line segments. The number of straight line segments used determines the number of springs and sliders needed to build the model. The spring constants may be determined by a relationship which involves the slope of the currBent line segment (m_n)

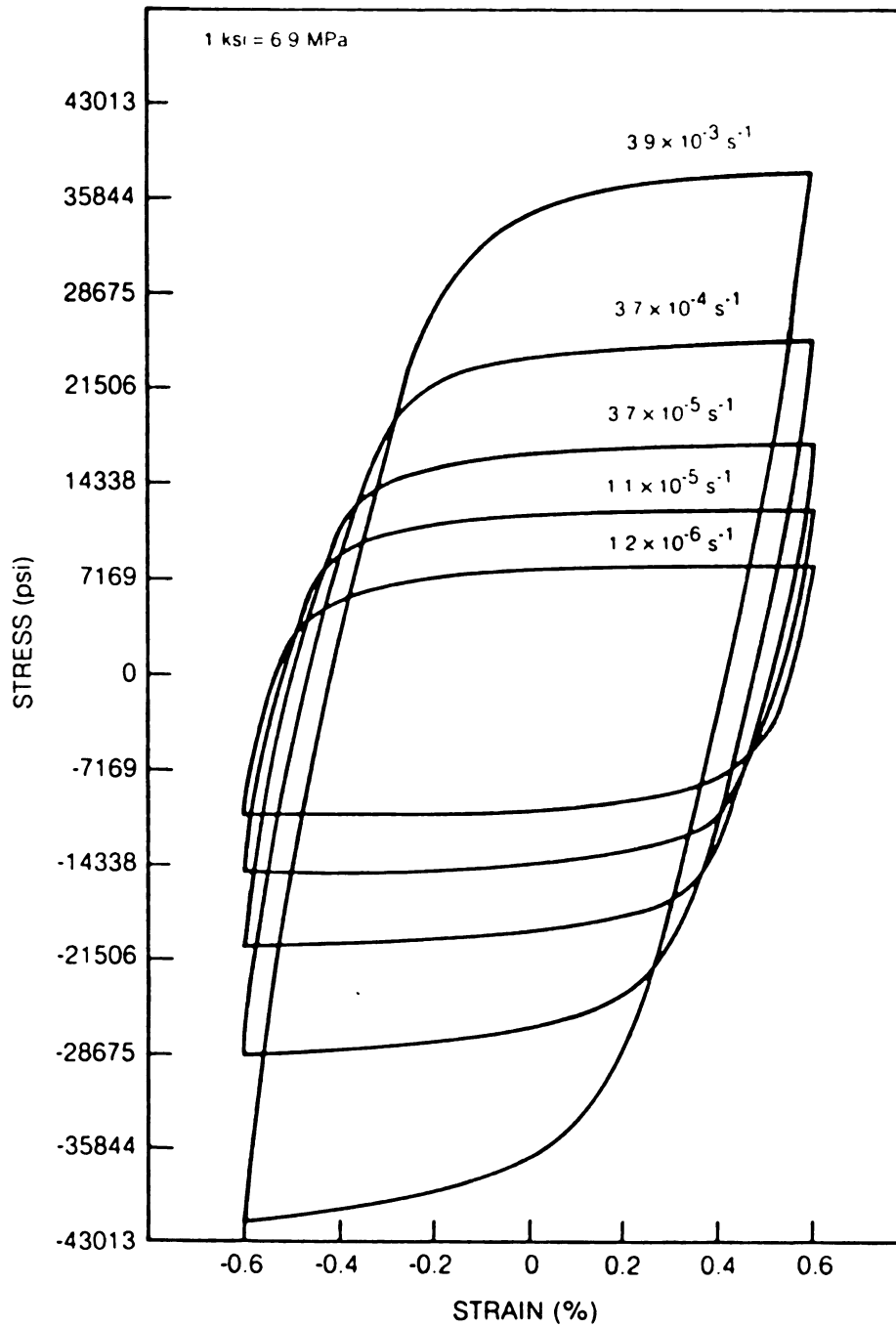


Figure 11: Stress-Strain Response of Cyclically Stable Hastelloy-X at 1600°F

a

d

te

t

ti

h

t

T

w

e

s

l

s

e

d

d

s

c

x

t

:

v

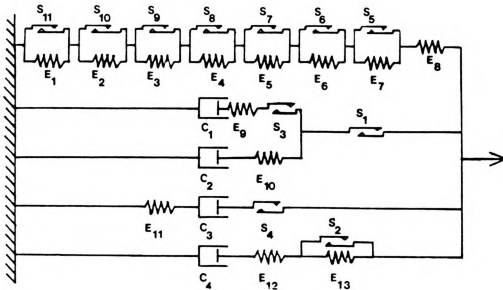
and the slope of the previous segment (m_{n-1}). The relationship is:

$$E_n = (m_{n-1}m_n)/(m_{n-1} - m_n)$$

The sliders used in the static model must be asymmetric to accommodate the greater stiffness of the material in compression than in tension. As a good approximation, all sliders are given the same initial asymmetry. The value of each slider will be one-half of the threshold value determined from the stable hysteresis loop shown. This halving of the values is required since each active slider is subjected to the complete allowable stress range during each cycle of loading. The modification of the static model to simulate the increased stiffness with higher strain rates is accomplished by adding groups of elements, each consisting of a viscous damper, a slider, and a spring connected in series and added in parallel with the existing model. The use of parallel groups is advantageous since each group experiences the same overall strain conditions, which is compatible with the data in terms of selected constant strain rates. The groups of parallel elements are determined by considering subsequently higher strain-rate loops and determining the parameters required to increase the effective dynamic stiffness of the model. The change in the initial slope of the curve, or the elastic modulus is adjusted directly by placing a spring of the required additional stiffness in parallel with the existing model. Since the spring must have negligible effect at the next lower strain rate, the new spring is placed in series with a viscous damper which will provide only a small stress at the lower strain rate. The viscous damper is sized to give the near constant change in stress observed at large strain values. The series combination of these two elements will

provide an increasing stiffness at increasing strain rates. Usually this increase in stiffness is much greater than that actually observed for strain rates higher than the loop being currently modeled. Therefore, a slider is placed in series with the combined spring and damper to limit the amount of stress which the combination will provide at the higher strain rates. The slider-damper series combination acts as a strain-rate trigger providing a release of the slider when the appropriate strain-rate is reached. This modeling approach provides a stress difference between the different strain-rate curves which initially is proportional to the strain level and asymptotically approaches a stress level of C_2 provided that this maximum value is less than the slider threshold value. More complex arrangements of elements could be devised to provide differences which vary in other ways. The final model, including the determined values of the various parameters, is shown in Figure 12. Notice that this model does not contain irreversible cyclic elements since the model is intended to be used to predict the stable response only of the material. Cyclic dampers are also not used here since the magnitude of the time-dependent creep causes the effect of cyclic creep to be negligible.

Whenever a collection of elements is added in parallel with the existing model, the response of the entire model at the lower strain rates is changed. This requires adjustment of the previously set model parameters. The amount of adjustment needed can be easily predicted with reasonable accuracy, thus reducing the number of iterations needed to produce a satisfactory model. In the case of the data used here, the difference in strain-rate is about one order of magnitude for all but one pair of loops. A difference of this size provides for an effect on



Model Parameters

Springs		Sliders			Viscous Dampers	
No.	E (ksi)	No.	S (ksi)	A	No.	C (ksi-sec)
1	17.2	1	9.70	-0.07	1	270000
2	669.2	2	7.00	0.0	2	150000
3	2245	3	3.40	-0.20	3	10000
4	2100	4	8.20	0.0	4	12000
5	5175	5	4.50	-0.14		
6	7960	6	6.20	-0.14		
7	28380	7	6.80	-0.14		
8	14190	8	7.55	-0.14		
9	3000	9	8.20	-0.14		
10	3100	10	8.56	-0.14		
11	4000	11	8.72	-0.14		
12	2800					
13	2400					

Figure 12: Model Representation of Cyclically Stable Hastelloy-X at 1600°F

previously set model parameters of about 10%. The single pair of loops which are spaced about one half order of magnitude apart would give rise to a 30% effect on the previous loop. Because of this, these two loops were modeled together and attached to a common slider as shown by S_1 in Figure 12. The use of interactive computer graphics is extremely helpful in this adjustment process.

The final output of the model compared with the data from which it was constructed is shown in Figure 13.

The second model to be constructed is that of Hastelloy-X at room temperature including the cyclic hardening observed during initial plastic straining of the material. This model will require the use of the irreversible cyclic elements. The data for this model was obtained by testing three smooth specimens with an axial extensometer at different strain rates with strain limits of ± 0.01 in all cases. The details of the testing procedures are discussed in Chapter 5. A representative stress-strain response is shown in Figure 14. Construction of the model is begun by developing the spring-slider model for the slowest strain-rate loop available as was done for the 1600°F model. The simplest technique of modeling the cyclic irreversibility found is by using a single cyclic irreversible element in parallel with the plastic response section of the static model. The elastic modulus of such a model will not change with cycling which is in agreement with the observed response. The irreversible element may be sized initially by noting the ratio of the maximum stress to the maximum stress of the first reversal. This value is noted to be 1.50. The maximum fraction of applied stress which the irreversible element must assume is then $1 - 1/1.50$ or 0.33. Since the fully developed element will assume .33

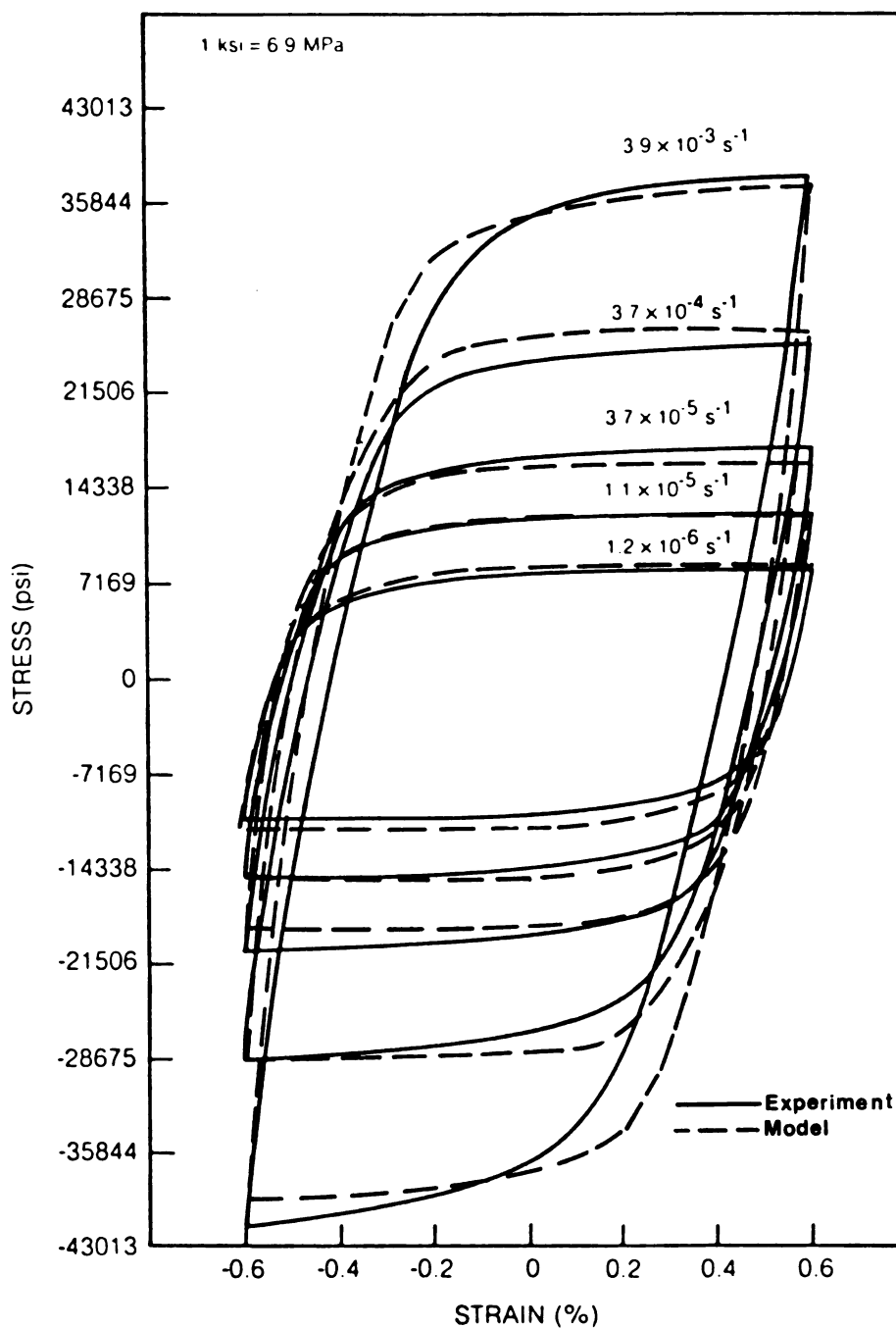


Figure 13: Comparison of 1600°F Hastelloy-X Model Response to Input Experimental Data

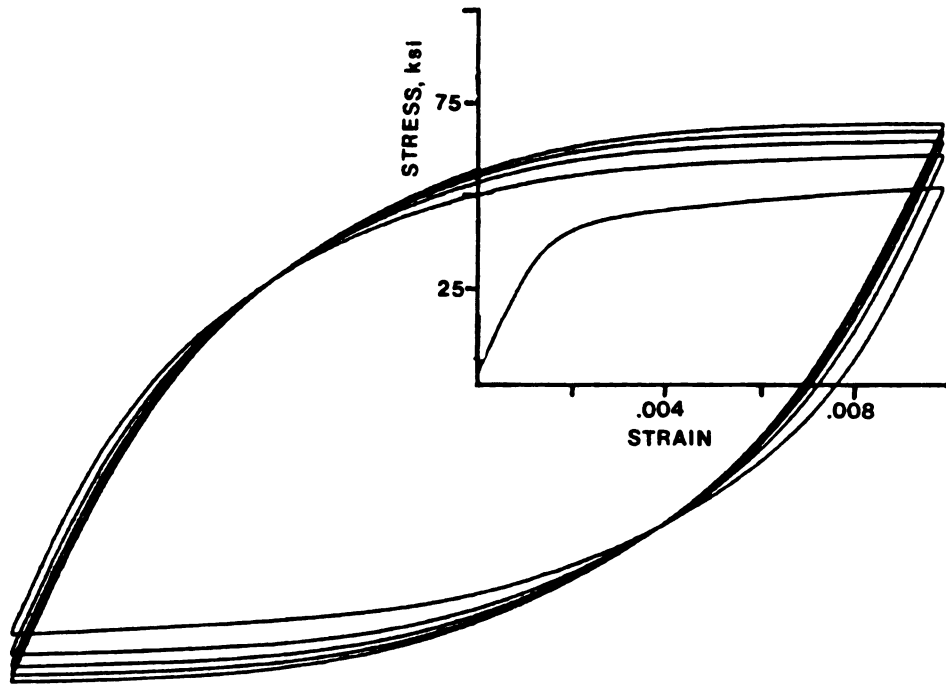
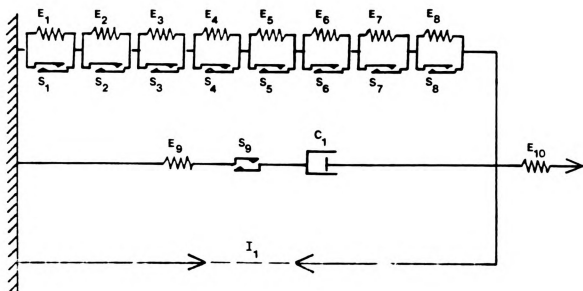


Figure 14: Initial Response of Hastelloy-X at Room Temperature Subjected to Constant Strain Rate Testing

of the total applied stress, the threshold values of all the sliders must be reduced by a factor of 0.67 to yield the correct response for a fully hardened specimen. The rate at which the irreversible element changes is expressed in half-lives of the element per reversal of loading. It can be seen from the data that the material is halfway between the first reversal and the stable response at about 7 reversals. The element must therefore experience .14 half-lives per reversal. These values are used in the model to provide a first try at cyclic hardening. The type of irreversible element used has been conceived to allow modeling of observed behavior with a minimum of elements, and frequently a single element such as this is sufficient. This initial model is then refined by interactively comparing the model output with the available test data and altering the model until good agreement is obtained.

The range of strain rates shown provides very little information concerning the time-dependent response of the material. Information to determine the time-dependent was derived by observation of the stress relaxation during the hold times involved in recording the various loops. By using the hold time and the total maximum relaxation of stress, a series combination of a spring, slider and damper may be determined. The slider value is one-half the observed maximum stress relaxation. The damper is sized to provide a suitable maximum stress at the lowest strain rate at which significant relaxation occurred. The spring constant is determined to allow the amount of relaxation to occur during the observed time. The model which results from this process and interactive adjustment is illustrated in Figure 15. The completed model does not incorporate cyclic dampers since the amount of relaxation of mean stress observed at room temperature is very small. The initial



Model Parameters

Springs		Sliders			Viscous Dampers	
No.	E (ksi)	No.	S (ksi)	A	No.	C (ksi-sec)
1	400	1	57.45	-0.04	1	10000
2	1985	2	54.47	-0.04		
3	4180	3	51.13	-0.04		
4	8930	4	47.70	-0.04		
5	11530	5	44.53	-0.04		
6	21210	6	39.56	-0.04		
7	31620	7	33.24	-0.04		
8	51110	8	22.40	-0.04		
9	30000	9	2.00	0.0		
10	20000					

Irreversible Cyclic Elements		
No.	I	R
1	0.34	0.14

Figure 15: Model Representation of Room Temperature Hastelloy-X

response of the model at the strain-rate of 0.0002 sec^{-1} including a short hold time at zero strain is shown in Figure 16.

The final model to be constructed is that of Hastelloy-x at 1200°F including the initial response. The construction of this model requires the use of all five element types available. Tests identical to those conducted for the room temperature modeling were done at 1200°F using a diametral extensometer. Certain difficulties arise in the construction of this model because the material exhibits a reversible, strain-rate-dependent, cyclic hardening and softening. If the material is stabilized at a given cycling rate, it will then restabilize to another response curve if the rate is changed. None of the five available modeling elements appear to provide this type of response. The five elements presented in Chapter 2 are not intended to represent a complete set of those available. Another element could be conceived to model this behavior. For the purpose of this example, two separate models will be constructed for Hastelloy-X at 1200°F . The first model will represent the response for the material stabilized at a low strain-rate (about 0.00002 sec^{-1}) and the second will represent the material undergoing rapid stabilization (strain-rate greater than 0.0002 sec^{-1}). The first model is constructed by determining the stable time-dependent model as was done at 1600°F . This model is then proportionately weakened to produce the first reversal of loading as was done for the room temperature model. An irreversible cyclic element is then added as in the room temperature model to cyclically stabilize the material to the proper level. The model is then complete since the relaxation of cyclic mean stress was not observed at this strain rate. The completed model is shown in Figure 17. The response of the model as

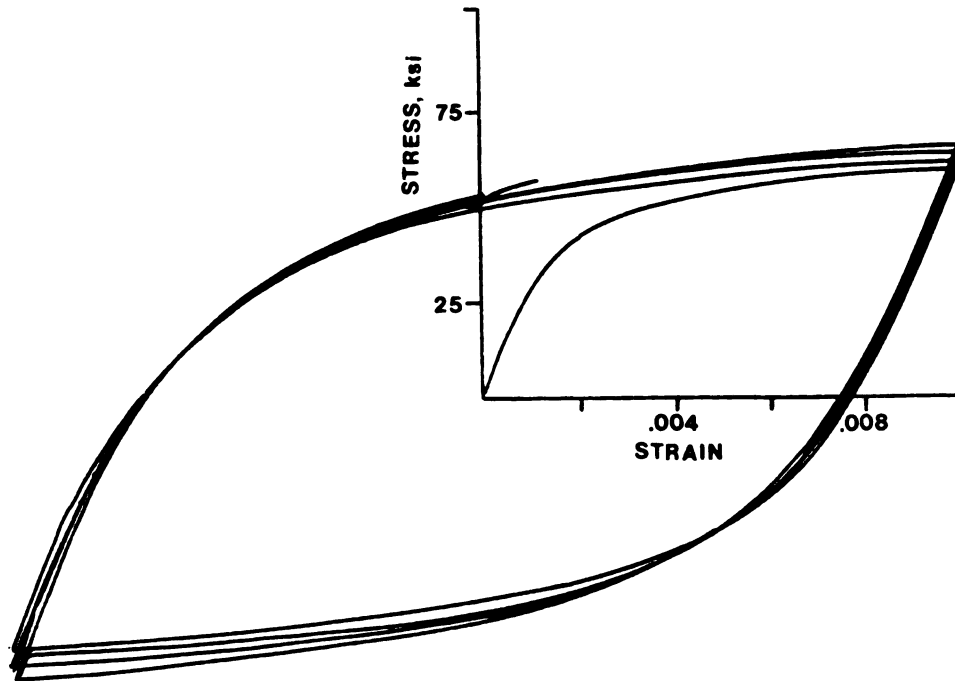
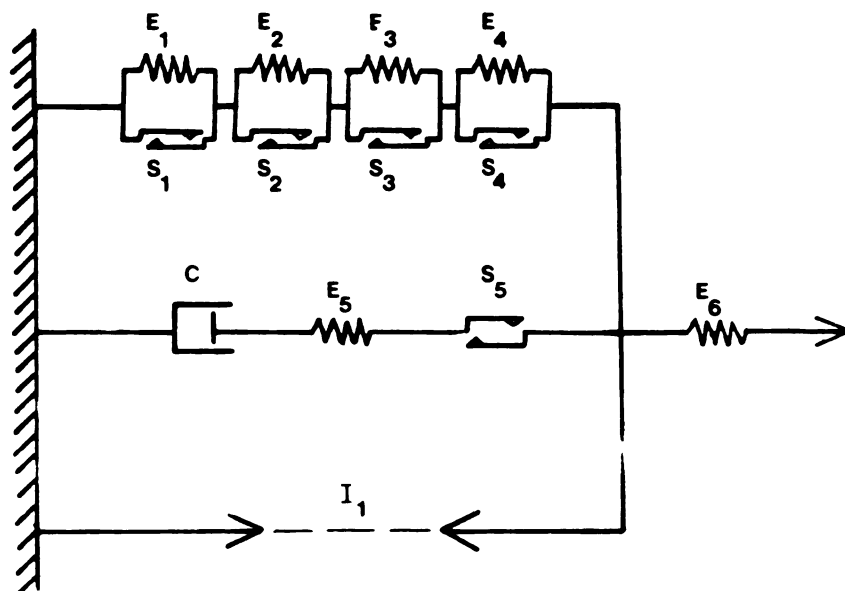


**Figure 16: Initial Response of Room Temperature Hastelloy-X Model
Subjected to Constant Strain Rate Testing**



Model Parameters

Springs		Sliders			Viscous Dampers	
No.	E (ksi)	No.	S (ksi)	A	No.	C (ksi-sec)
1	542	1	33.7	-0.04	1	200000.
2	3400	2	30.4	-0.04	Irreversible Cyclic Elements	
3	11800	3	24.2	-0.04		
4	46700	4	16.2	-0.04		
5	23100	5	5.0	0.0		
6	40000					
					No. I R	
					1	0.46 0.20

Figure 17: Model Representation of 1200° Hastelloy-X at Low Strain Rates

compared to typical input data is shown in Figure 18.

The model for the more rapid strain rate is constructed in a manner identical to the slow response, with the exception of the use of irreversible cyclic elements and the addition of cyclic dampers. The single irreversible cyclic element used in the previous two models is not capable of producing the cyclic hardening observed here. The material begins to harden very rapidly at first and then quickly reduces the rate of hardening and continues at a much more constant rate for an extended number of cycles. This behavior can be achieved through the use of two irreversible cyclic elements in parallel. The first element hardens very quickly to produce the initial response while the second element changes much more slowly to provide the more constant hardening rate observed later. The specific constants for the two elements was determined by trial and error with the single constraint that the sum of the maximum strength coefficients must be the value that would be used for a single element.

The determination of the cyclic damper was done in such a way as to provide the approximately 6 ksi maximum relaxation observed on a strain amplitude of 0.01 without strengthening the entire model by that amount. The required damper was placed in parallel with the spring slider pairs which provide the static plastic response and the sliders were weakened appropriately to account for the strengthening effect of the damper. Figure 19 is a schematic of the completed model. Figure 20 is a comparison of the model response with the experimental results of a test showing the cyclic relaxation of mean stress. Notice that the reduction in the change from one cycle to the next in the maximum stress attained is very similar in the two cases. The similarity in the shape of the

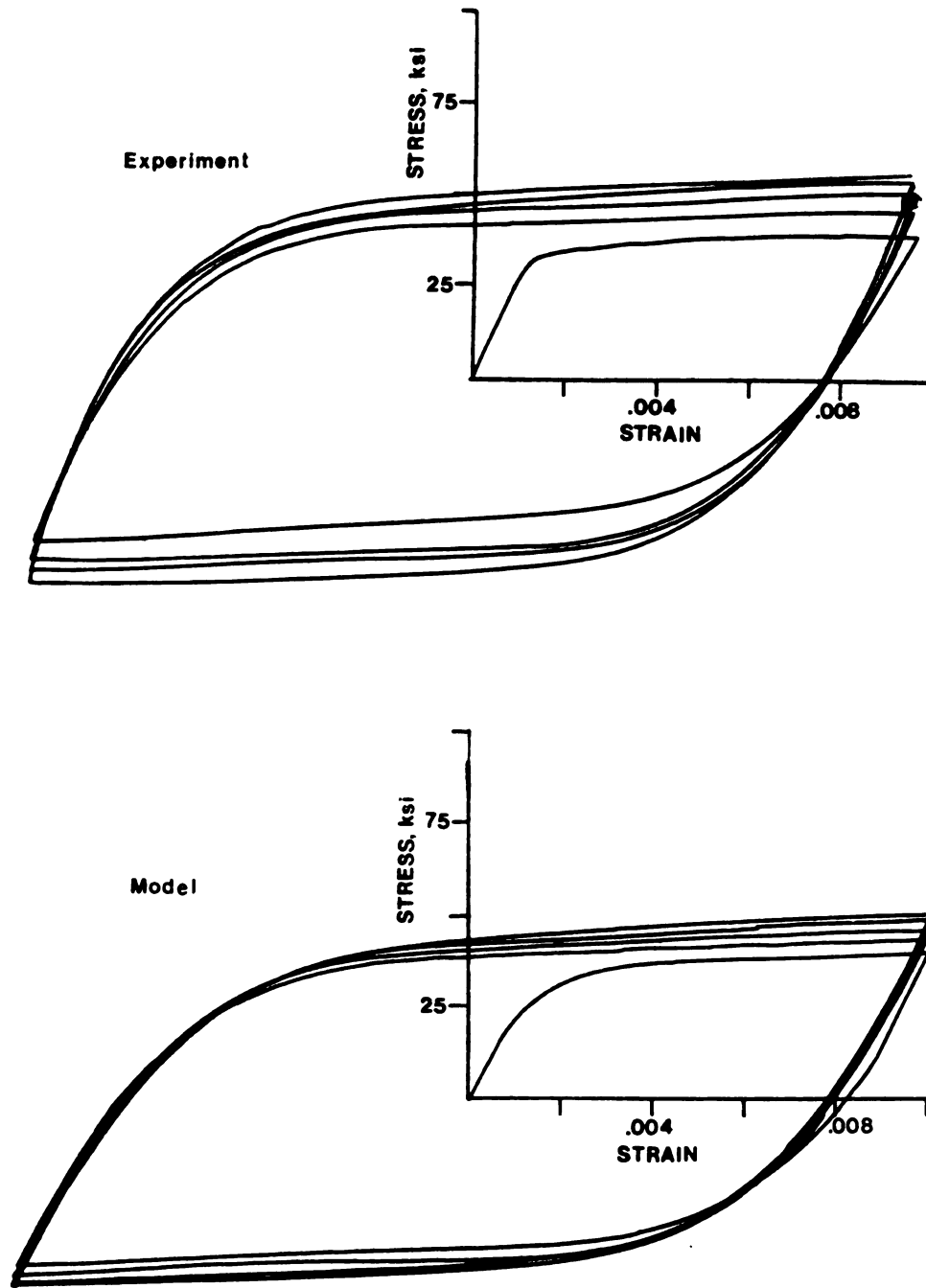
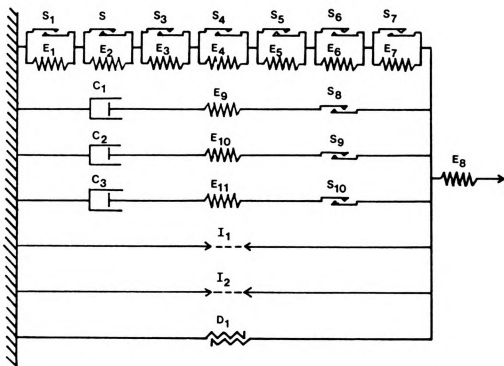


Figure 18: Comparison of Model and Experimental Response for Hastelloy-X at Low Strain Rates



Model Parameters

Springs		Sliders			Viscous Dampers	
No.	E (ksi)	No.	S (ksi)	A	No.	C (ksi-sec)
1	1380	1	24.1	-0.01	1	200000
2	3700	2	28.5	-0.01	2	15000
3	6730	3	27.2	-0.01	3	1000
4	13300	4	25.4	-0.01		
5	22000	5	22.3	-0.01	Cyclic Dampers	
6	46600	6	18.6	-0.01		
7	114000	7	10.8	-0.01	No.	D (ksi-reversals)
8	27200	8	5.0	0.0	1	600
9	40000	9	3.0	0.0		
10	10000	10	2.0	0.0		
11	200					

Irreversible Cyclic Elements

No.	I	R
1	.174	.548
2	.406	.072

Figure 19: Model Representation of 1200°F Hastelloy-X at Rapid Strain Rates

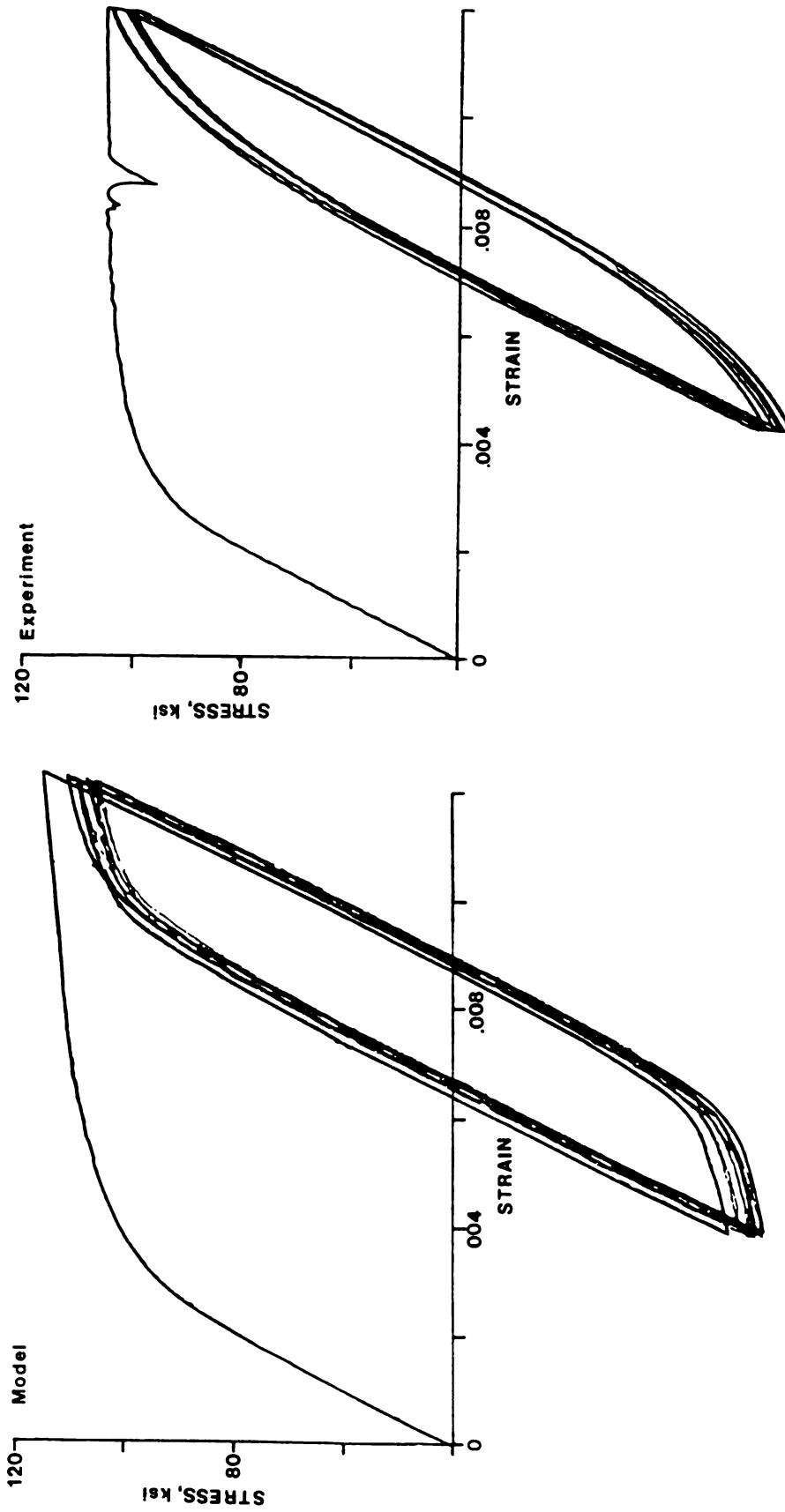


Figure 20: Comparison of Model and Experimental Relaxation of Cyclic Mean Stress

two hysteresis loops is not as great. This lack of similarity is caused by the determination of irreversible cyclic elements based on the peak stresses of the input loops. Better agreement could be achieved by the incorporation of irreversible cyclic elements in parallel with smaller portions of the plastic response. The effect of these additional elements on the large strain range response would be small.

4.5 Other Model Construction Techniques

The examples of model determination in the last section have primarily been conducted from a basic knowledge of the reaction of the various elements in simple configurations and the addition of simple subsystems to develop the models. These techniques are very useful because they produce physically meaningful models with readily predictable behavior. The generalized modeling technique is capable of handling much more complicated model arrangements.

The change in stress observed at a range of strain levels for various strain rates does not necessarily have a decreasing slope with increasing strain at all points and may not be monotonically increasing. In such cases, no actual combination of springs and viscous dampers can fit the input data. The use of springs and dampers with negative coefficients can be used to develop a specific model which will provide the observed response. These combinations may also be helpful in modeling a negative strain-rate sensitivity. The effect of such elements on an existing model can be difficult to predict and it is suggested that some experimentation with simple example models be conducted to gain insight into this behavior.

The models constructed have been presented in simple schematic

figures. Much more complicated element connection geometries may be analyzed which would be difficult to illustrate with such simple figures. These complicated geometries may be of considerable use in modeling certain behavior. Such models could contain extensive cross-connections, making visualization of the response extremely difficult. Again example models of such types should be used to gain insight concerning this type of model.

CHAPTER 5

DESCRIPTION OF EXPERIMENTAL EQUIPMENT AND PROCEDURES

5.1 Test Equipment Description

This chapter provides a brief description of the closed-loop test system, diametral gage, and interferometric strain gage used in the test program. Information is also included concerning the signal conditioning required to obtain the required output from the tests. The specimen geometries are also described.

A computer controlled, MTS closed-loop hydraulic testing machine was used to perform all tests. The heating of the specimen was done with an induction furnace using multiple turn, water cooled, copper coils. The specimen temperature was controlled through a modulating feedback control system receiving its signal from a thermocouple, spot welded to the specimen in the region of interest, similar to that done by Lucas [18]. The machine grips were water cooled to protect the load cell and prevent melting of the lower Wood's metal type grip and to provide a flat temperature profile at the center of the specimen.

The elevated temperature testing of nominal response and generation of data for model construction was done with a diametral extensometer. The extensometer is similar to that used by Slot [31] and Lucas [18] which employs a ceramic contact device and an invar fulcrum to minimize the effect of temperature changes on the gage response. The diametral displacement was converted to axial strain by means of an analog circuit. This circuitry requires that either the initial elastic modulus or

the elastic Poisson's ratio of the material be known to determine the axial strain from the extensometer output. A detailed discussion of this procedure is found in reference [31]. In this particular case Poisson's ratio was chosen as the known value since the temperature dependent variation is less than that of the elastic modulus [32].

The measurement of notch root response was done with the interferometric strain gage. This gage is capable of measuring strains at room and elevated temperatures (above 1200°F) over a gage length of 100 microns (.004 inches). The gage is based on the use of interference patterns formed by the diffraction of coherent light from two closely spaced indentations. The movement of these patterns is a direct measure of the change in spacing of the two diffractive points. Detailed descriptions of the gage theory and operation have been written by Bofferding [17], Lucas [18], and Sharpe [23,24]. The gage used in these tests is identical to that described by Lucas[18]. The reflective surfaces are formed by a pyramidal diamond indenter using a Vicker's microhardness tester as described by Lucas [18].

5.2 Specimen Geometry

Three specimen geometries were used in the various phases of testing. A straight, smooth specimen was used with a .300 inch axial extensometer to determine nominal material response at room temperature. A detailed drawing of the specimen is presented in Figure 21. An hour-glass shaped specimen was used for nominal elevated temperature response in conjunction with the diametral gage. This specimen provides a minimum cross sectional area at a single point where the extensometer is positioned. A detailed drawing of the specimen is shown in Figure 22.

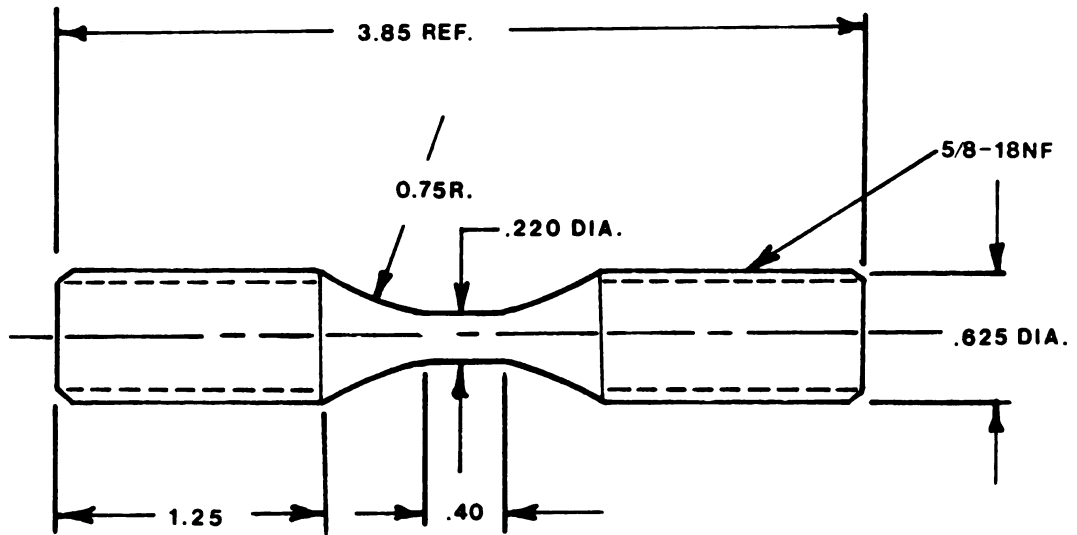


Figure 21: Smooth Axial Test Specimen Geometry

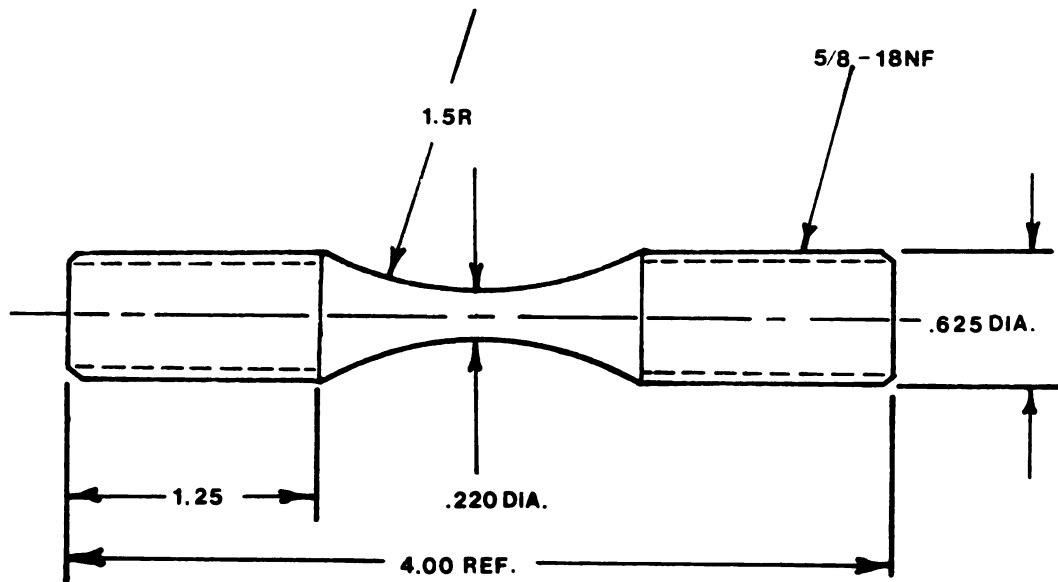


Figure 22: Hourglass Shape Diametral Specimen Geometry

The circular and elliptical notched specimens were used with the interferometric strain gage at both room temperature and 1200°F to provide the local response at a known stress concentration value. Figure 23 is a detailed drawing of the notched specimens. The two types of notched specimens were identical with the exception of the geometry of the particular notch.

5.3 Test Procedures

The nominal room temperature response was recorded by conducting tests at three different strain rates with a strain amplitude of ± 0.01 . The rates were chosen such that one complete strain cycle required 20, 200 and 2000 seconds to complete. Representative results of these tests are presented in Figure 14. Three different specimens were used such that the time dependence of the initial behavior of the material could be observed. Following the completion of each test, a single complete strain cycle was run and recorded at each of the three rates to provide a control response for comparison between the three specimens. The amount of stress relaxation observed and the time required was noted at the zero strain point on some of the strain cycles. This was done to provide additional information concerning the time-dependent response of the material. A final variable-strain-rate test was run on a fourth specimen to be used to compare to the response of the model constructed from the constant-strain-rate tests. The specifics of this test are presented in Chapter 6.

The room temperature test to measure notch root strain was conducted on an elliptical notched specimen. Symmetric cyclic loading at a constant load rate was used for the test. Details of the load input and

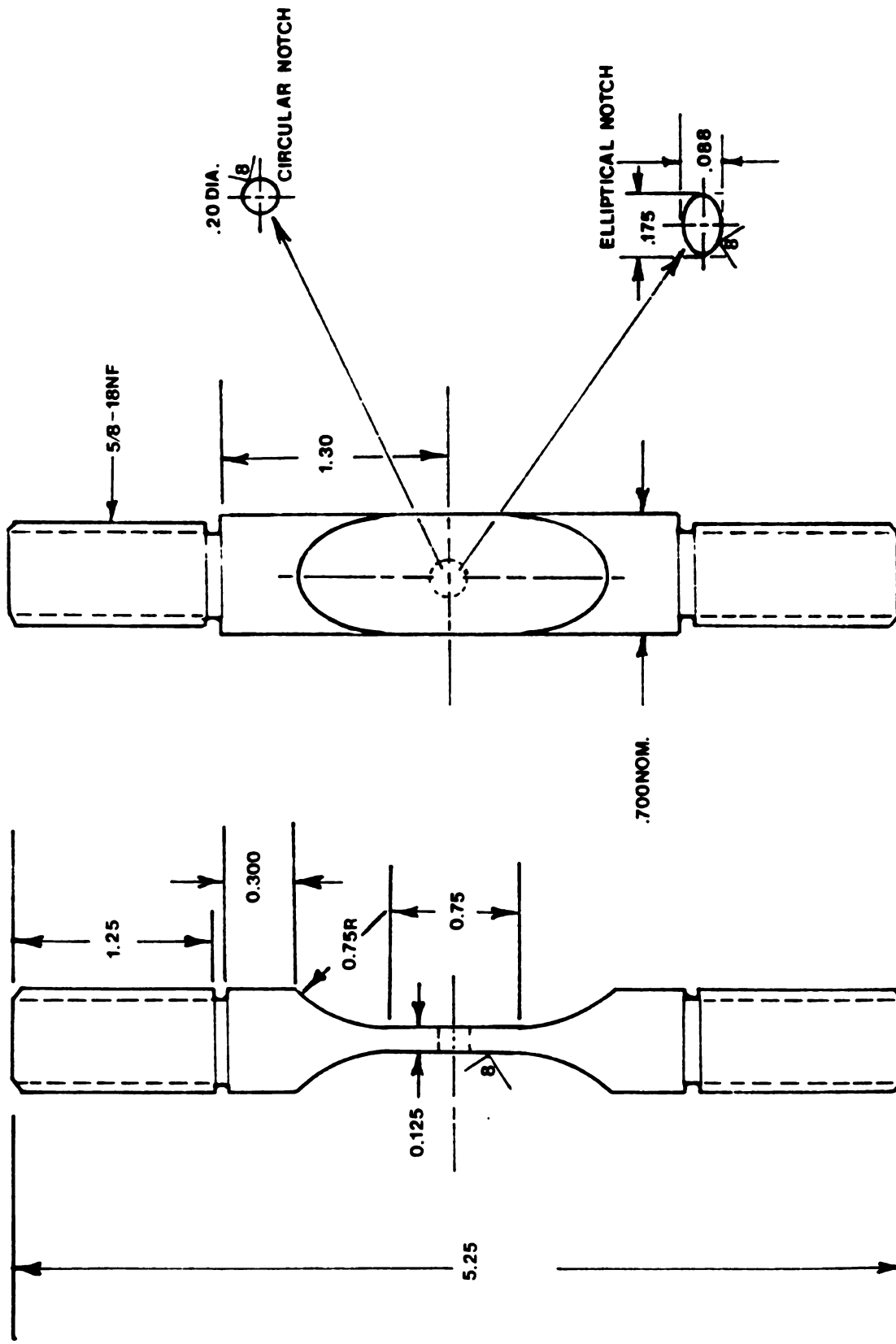


Figure 23: Notched Specimen Geometry

the results are contained in Chapter 6.

The nominal response at 1200°F was determined using the same series of tests as at room temperature described above. One additional test was conducted at this temperature to determine the cyclic relaxation of mean stress of the material. A similar test at room temperature showed only a very small relaxation. Representative results of the testing are presented in Figure 18. The notch root response information for this temperature was taken from Lucas [18]. Details of the data used are presented in Chapter 6.

The 1600°F testing consisted of verifying the data presented by Walker [28] to assure the reliability of further tests and conducting a variable strain-rate test for comparison with the model in Chapter 6.

CHAPTER 6

COMPARISON OF EXPERIMENTAL DATA TO THE MODEL RESPONSE

6.1 Introduction

This chapter presents several comparisons between the response of the models constructed in Chapter 4 and the results of specific experimental testing as described in Chapter 5. The comparisons to be made include that for variable strain rate tests at room temperature, 1200°F, and 1600°F; and notch root strain response for cyclic load controlled tests at room temperature and 1200°F. All tests and comparisons are made using Hastelloy-X specimens. The test results are presented below, grouped according to the particular model used to predict the material response.

6.2 Comparisons at 1600°F

The testing at 1600°F was done on a cyclically stable specimen. The input for the strain controlled test is illustrated in Figure 24. The material model determined in Chapter 4 was subjected to the same input.

The comparison of the two responses is presented in Figure 25. The maximum discrepancy between the two responses is about 5 ksi or 9% of the total stress range experienced. The major differences between the two occurs during the times of stress relaxation. Some similar discrepancies may be observed when comparing the model response with the input data. A model which would provide better correlation with the input

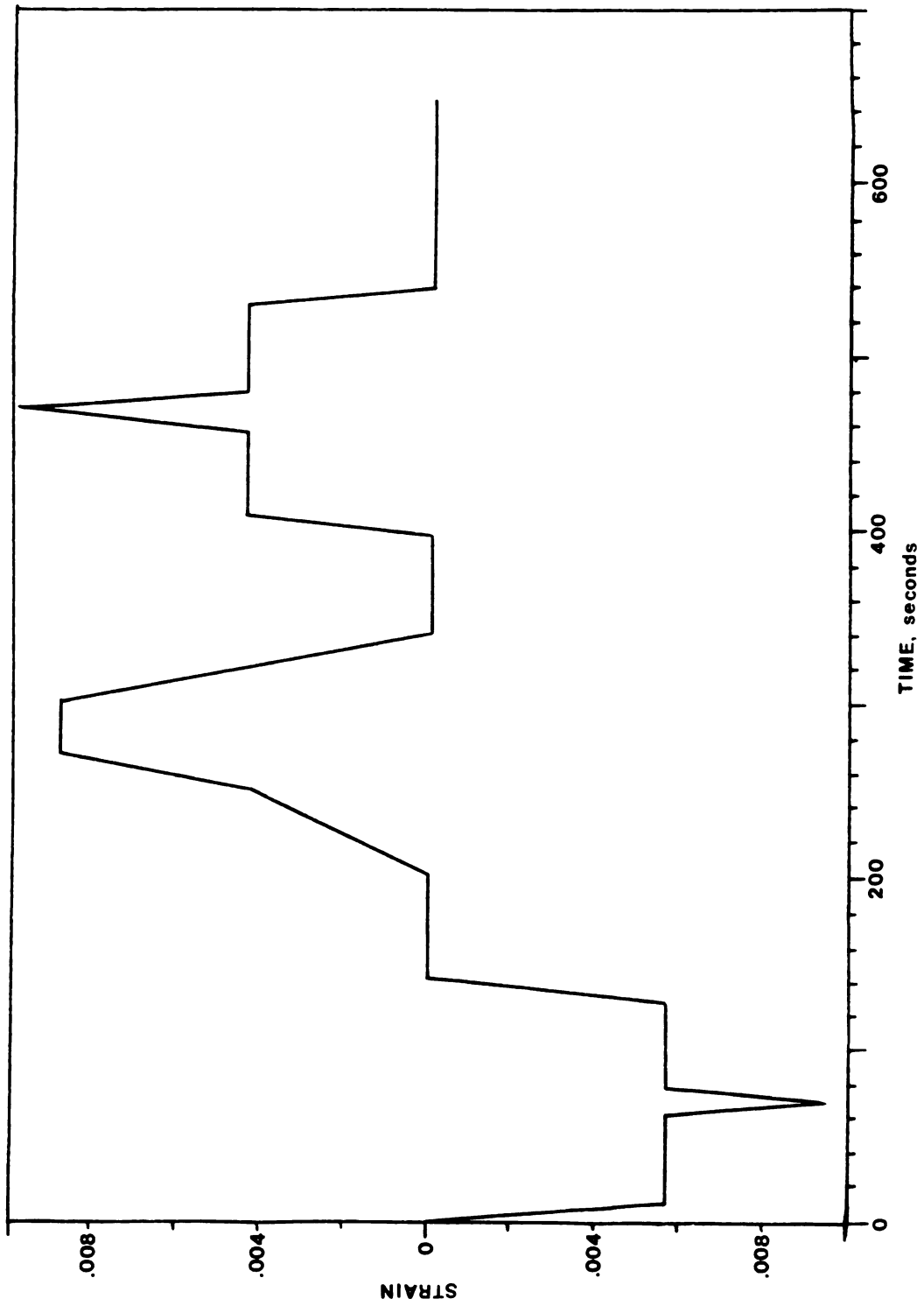


Figure 24: Variable Strain Rate Input for 1600°F Test

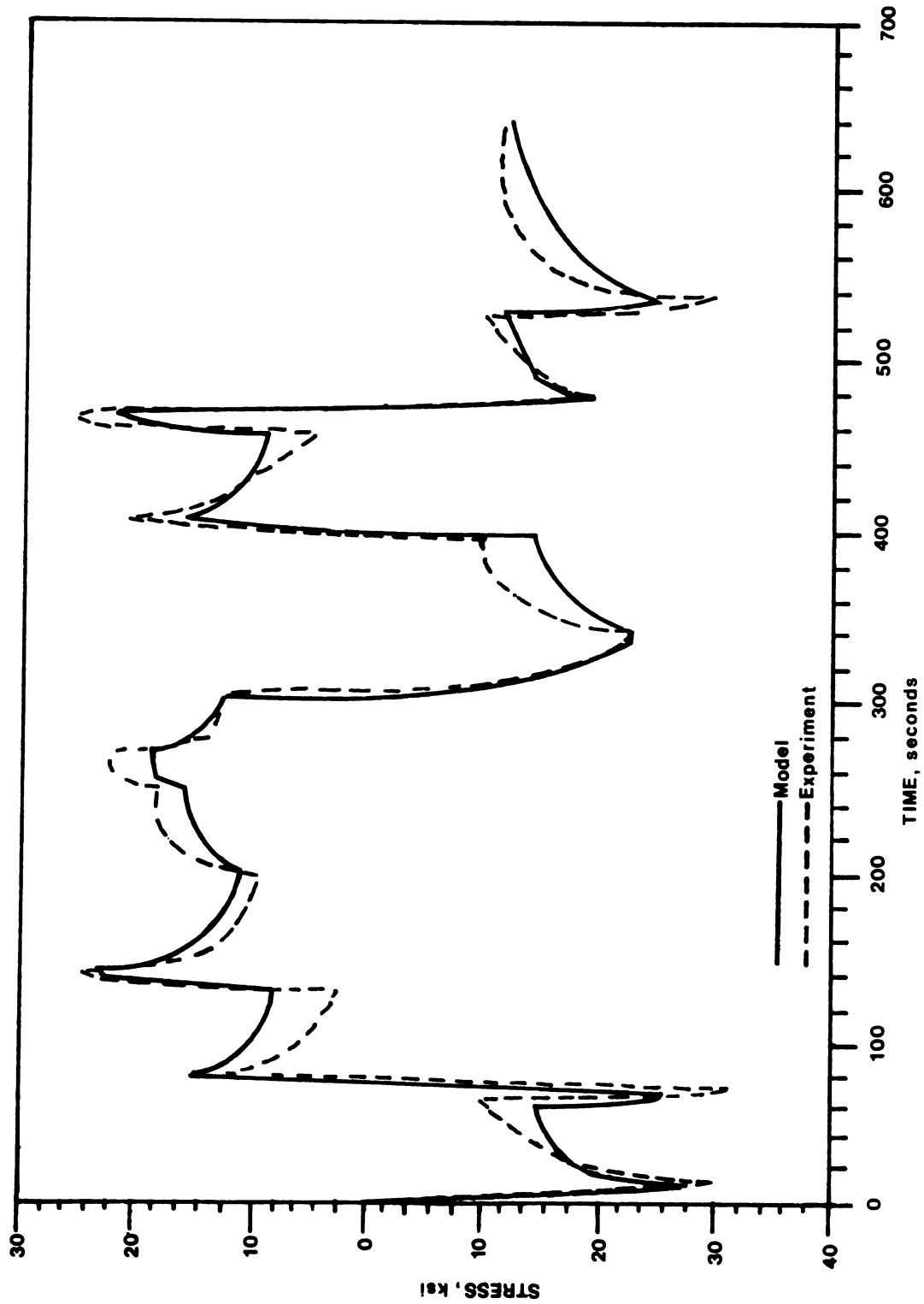


Figure 25: Comparison of Model and Experimental Response for 1600°F Test

data should reduce the amount of error observed here. Considering the amount of time-dependent creep observed in this test, the degree of agreement that the model response exhibits with the experimental result is very good.

6.3 Room Temperature Comparisons

The first room temperature test is similar in structure to the 1600°F test explained above. In this case, the specimen is in the initial state and experiences cyclic hardening during the test. The input strain history for the test is shown in Figure 26. The comparison between the model and experimental response is presented in Figure 27.

The degree of difference between the two responses is no more than 4% of the total stress range of the test. The agreement in the amount of stress relaxation is exceptional considering the source of the data for determination of the viscous damping coefficients in the model.

The second room temperature test is the comparison of the notch root strain response of an elliptical notch specimen subjected to controlled load cycling. The load cycling was a constant load rate with an amplitude sufficient to provide a nominal stress of ± 28.57 ksi with a period of 40 seconds. The model response requires the determination of an elastic stress concentration factor to be used in the Neuber analysis. This concentration factor was determined experimentally using the interferometric strain gage in the same configuration as was used to determine the notch root response during the test. The experimentally determined factor for a small, completely elastic load was 3.54. This factor is considerably lower than the theoretical value of 5.2 published by Peterson [29]. The experimentally determined value was used here

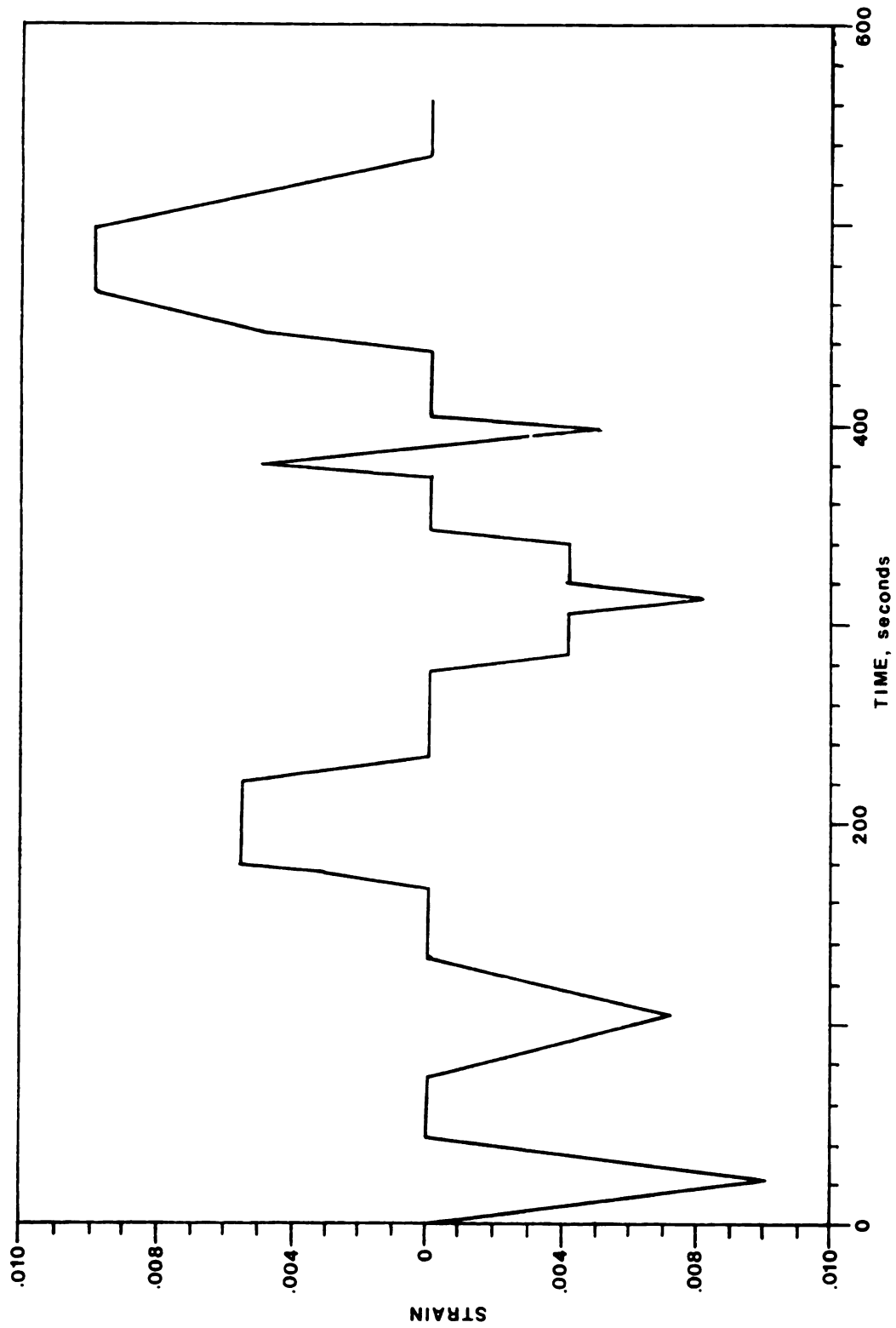


Figure 26: Variable Strain Rate Input for Room Temperature Test

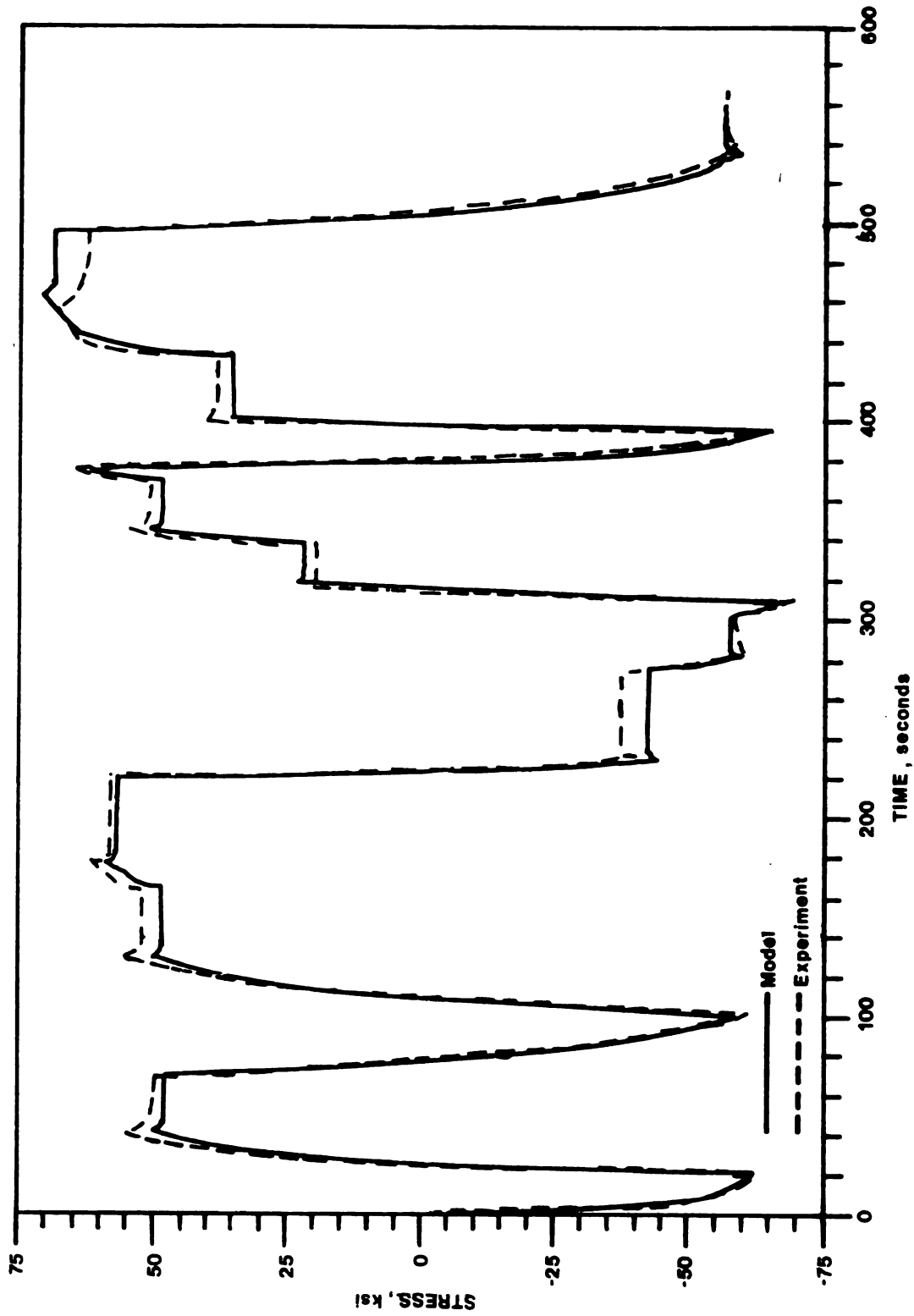


Figure 27: Comparison of Model and Experimental Response for Room Temperature Test

since it is considered to be more representative of the particular experiment.

The comparison between the experimental and model response is presented in Figure 28. The agreement between the two data sets is quite good in this case. The use of a somewhat higher value of k_t would yield results which agree extremely well with the observed response since the shapes of the two response curves shown are nearly identical.

6.4 Comparisons at 1200°F

The nominal response testing at 1200°F consisted of a test similar to that performed at 1600°F with the exception of the duration of the test. The test was conducted over a relatively long time period to allow large amounts of time-dependent response. A plot of the strain versus time input used in this test is shown in Figure 29. The model constructed to predict response at slow strain rates was used in this case. The results of the comparison are presented in Figure 30.

In general, the agreement between the two responses is very good. A large discrepancy does occur during the last two positive stress areas of the test. This discrepancy is possibly caused by the use of only a single irreversible cyclic element to determine the cyclic hardening. The error experienced here is still within 15% of the total stress range of the test and is considered very good for the simplicity of the cyclic hardening portion of the model.

The final test is that of the strain response of a circular notched specimen at 1200°F subjected to regular cyclic load cycles with hold times at the cycle peaks. The load range is sufficient to produce a nominal stress range of ± 34.7 ksi. and is applied at a constant loading

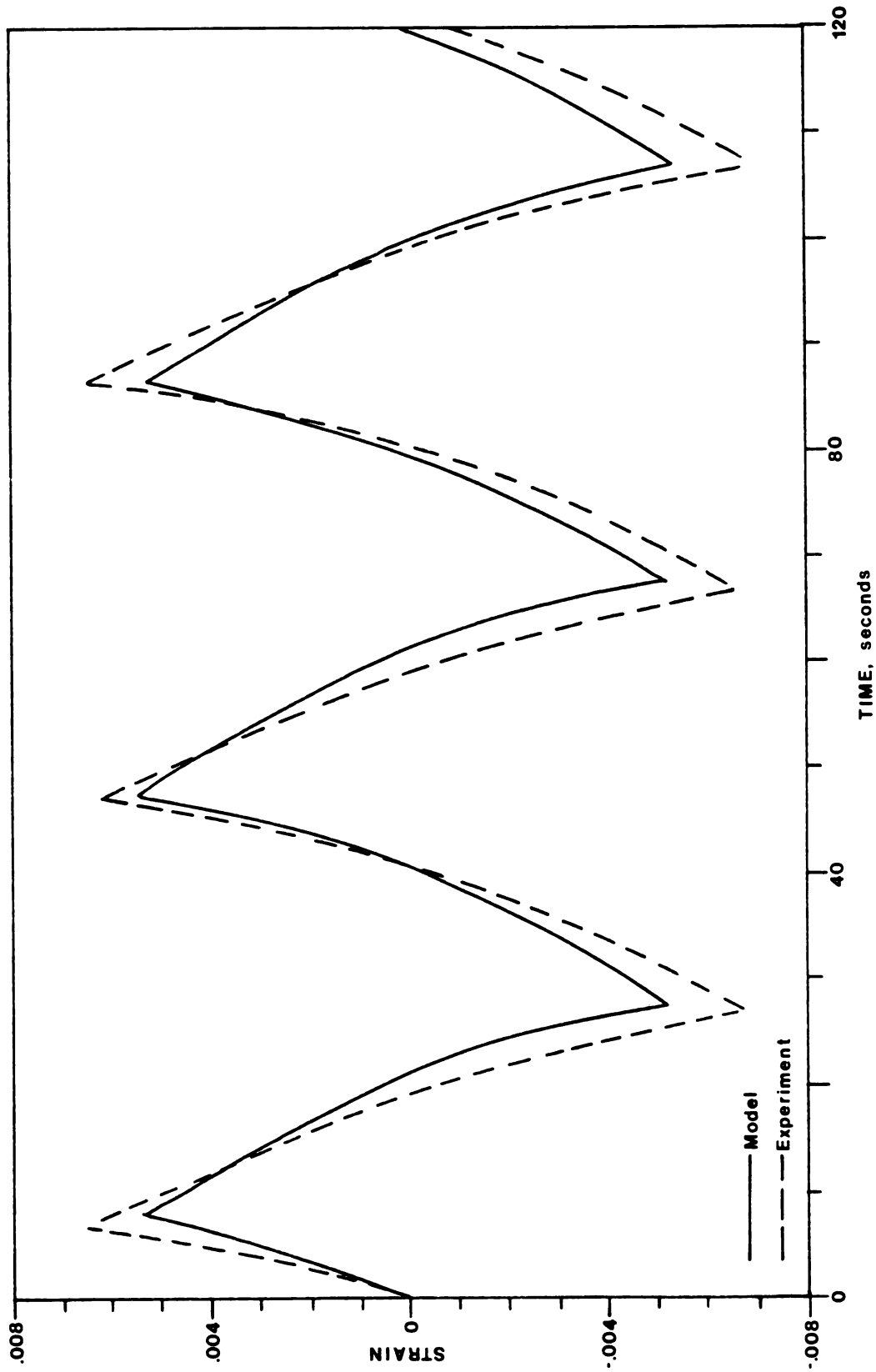


Figure 28: Comparison of Model and Experimental Notch Root Response for Room Temperature Test

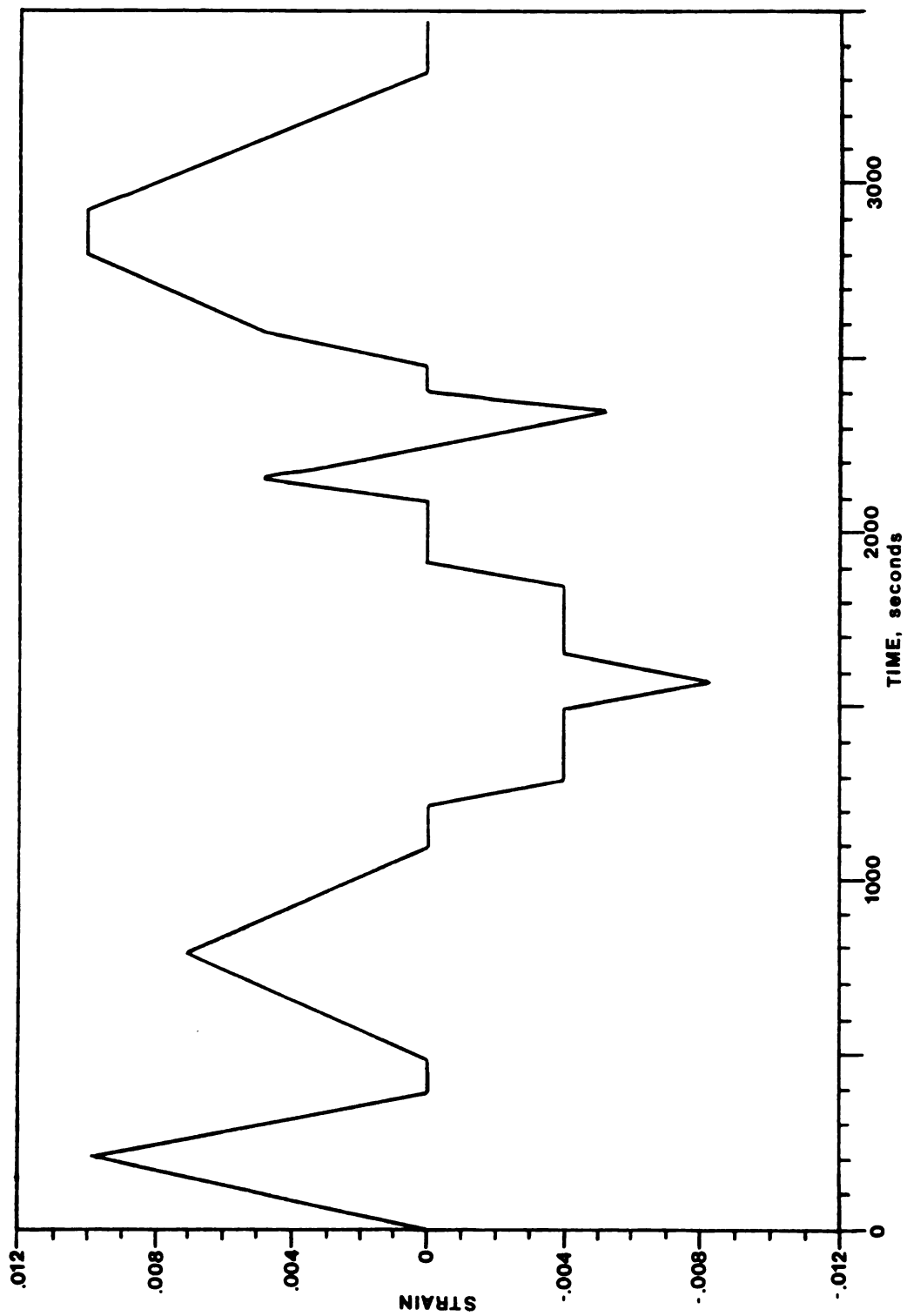


Figure 29: Variable Strain Rate Input for 1200°F Test

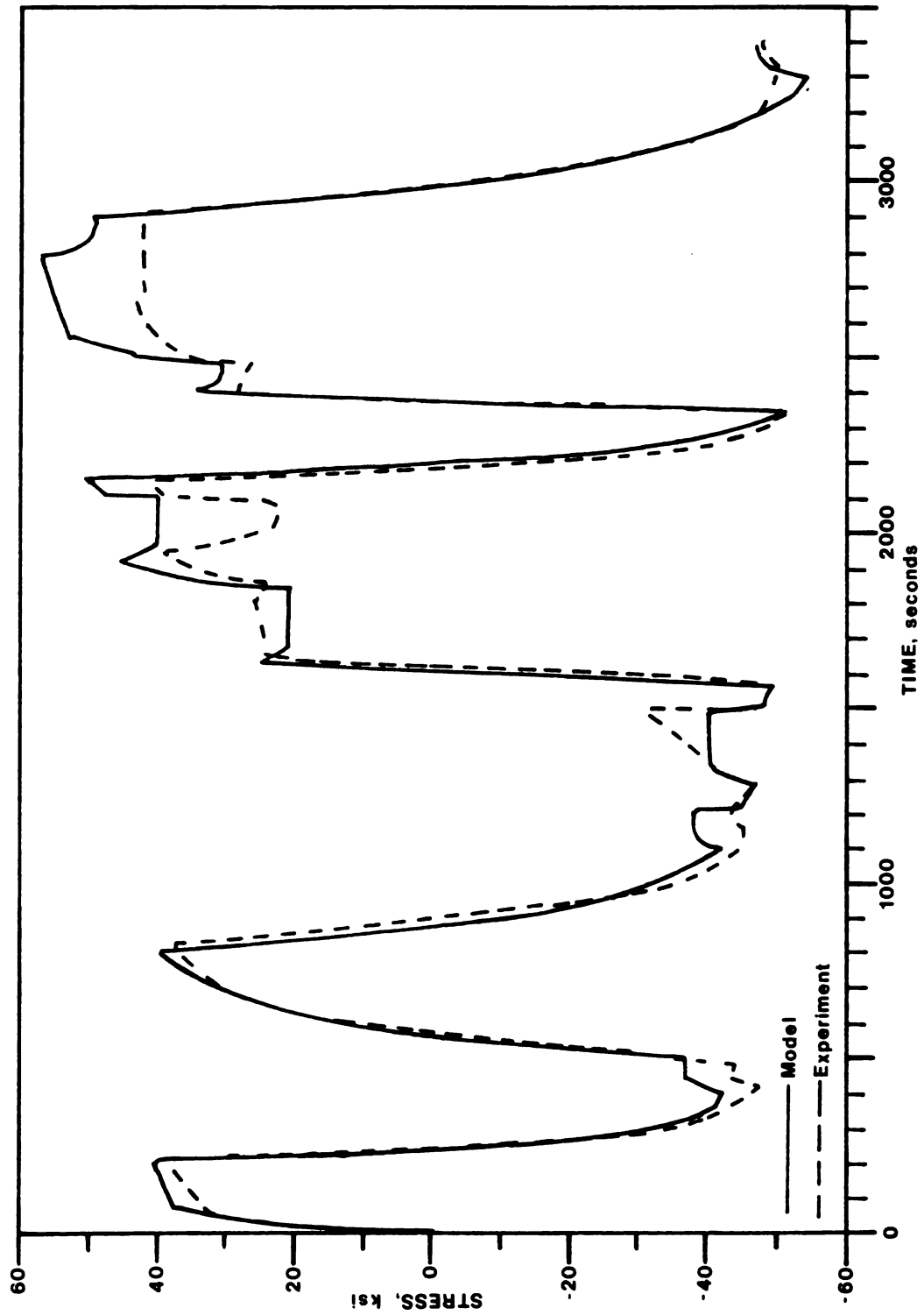


Figure 30: Comparison of Model and Experimental Response for 1200°F Test

rate to require 20 seconds peak to peak. At each peak a hold time of 100 seconds exists. The elastic stress concentration factor was again derived from the experimental results and determined to be 2.27 by Lucas [18] for the net section or 3.18 for the gross section as compared with the theoretical value of 3.3 published by Peterson [29]. The model used in this test was the one designed for strain rates greater than $.0002 \text{ sec}^{-1}$. The comparison of the experimental and model response for this test is shown in Figure 31.

The results of the comparison show very good agreement between the two with the general form of the response being very close to the measured output. The major discrepancy is in the magnitude of the strains predicted. The model strain values are within 18% of the experimental values at all places during the test. Again, the use of a higher stress concentration factor would provide excellent agreement between the observed and predicted responses. In both Neuber simulations, a higher stress concentration factor would provide better agreement and the theoretical stress concentration factors give support to the use of a higher value.

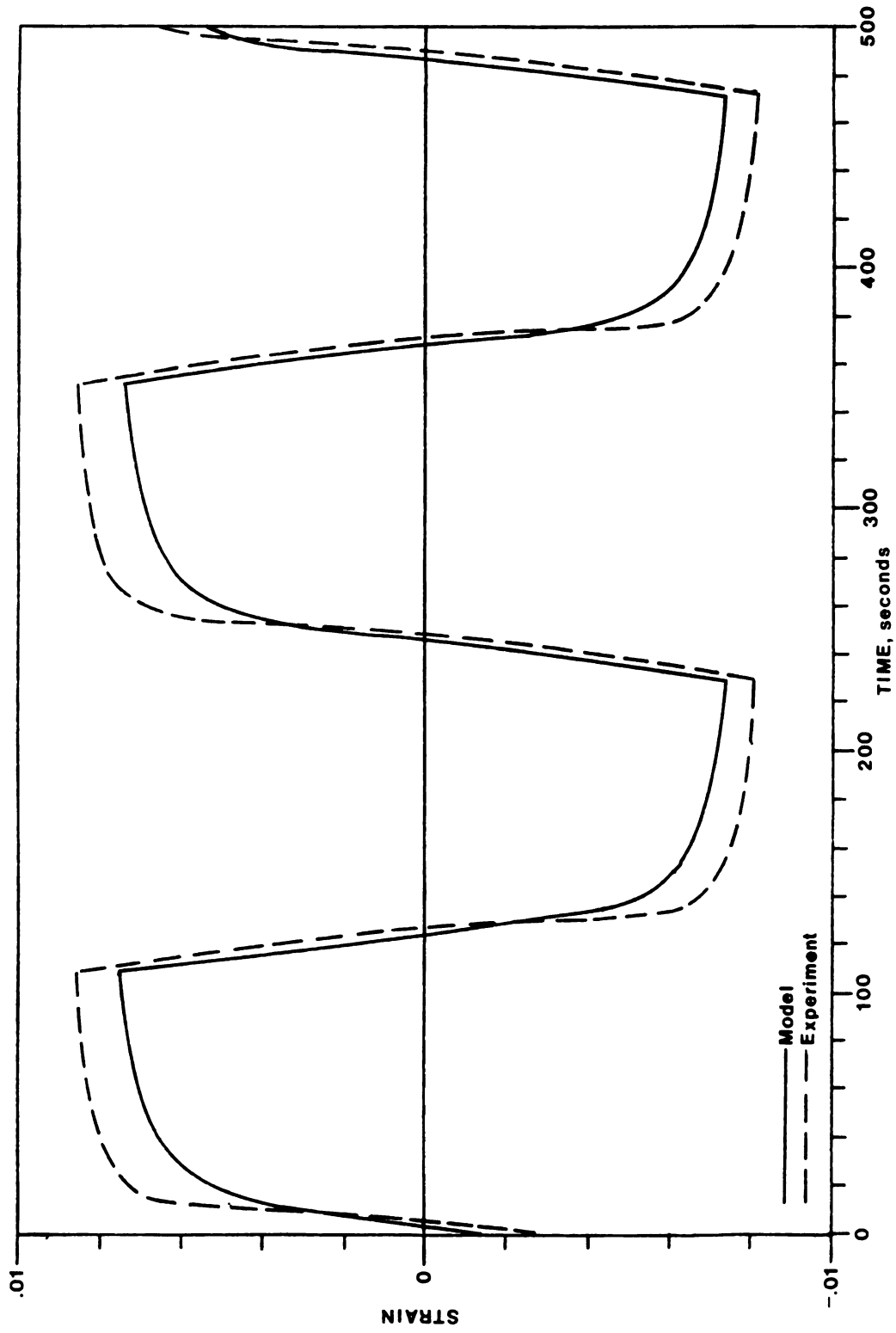


Figure 31: Comparison of Model and Experimental Notch Root Response for 1200°F Test

CHAPTER 7

CONCLUSIONS AND DISCUSSION

It is shown that a generalized constitutive modeling technique can be formulated using a matrix approach similar to that used in discrete vibration analysis. With this technique, classical rheological model elements consisting of linear springs and viscous dampers can be combined with frictional sliders and two new special purpose model elements to simulate cyclic hardening or softening, cyclic relaxation of mean stress, history dependent memory, time-dependent creep and time-dependent stress relaxation. Because of the versatility of this new method for creating this type of constitutive model, various arrangements of classical and special model elements can be experimented with to develop a particular model that can simulate both cyclic and time-dependent behavior, that is appropriate for a particular class of materials.

Notch root behavior is also successfully modeled by developing a numerical technique for incorporating the generalized constitutive model into the Neuber relation. Notch root stress-strain response could then be predicted from known nominal stress or strain histories.

Uniaxial behavior is modeled for Hastelloy-X at room temperature, 1200°F and 1600°F. Isothermal tests that isolated individual phenomena such as cyclic hardening were performed to determine the needed material properties. Additional tests were conducted that exhibited combinations

of both time-independent and time-dependent behavior for the specific purpose of determining the accuracy of the model. All the model predictions followed the general trend of the experimental verification data. The best correlation was for room temperature. Second best correlation was at 1600°F and the largest errors were seen at 1200°F. Hastelloy-X is difficult to model at 1200°F because of the lack of a dominant behavior that is either time-independent or time-dependent. This necessitated the interaction of all model elements simultaneously for an accurate prediction.

Some limitations to the modeling technique were encountered owing to the lack of the availability of certain types of elements that were needed to simulate some of the unusual phenomena observed under cyclic loading at elevated temperatures. It should be noted that the five elements presented here are not intended to be a complete set. This general modeling technique allows for the addition of other types of special purpose elements that could be used to model other materials that behave very differently. The incorporation of the Neuber relation into the modeling technique has been shown to provide an accurate technique for the determination of notch root stress-strain response.

The primary difficulty encountered in using this technique has been the determination of the configuration of the constitutive model which best fits the available experimental data. The technique used in model building to this point is subjective with a rationale that was based on a knowledge of the specific properties of the elements available. The extensive use of trial and error is also employed. The development of a method for establishing the required input data to produce a complete model would also be extremely beneficial.

The present work deals entirely with uniaxial response of the material. The possibility exists for extending the technique to multiaxial response. Such an extension will introduce extreme complications into the materials models. A single elastic spring representing linear behavior in one dimension becomes four springs for two-dimensional representation, one of which is negative, and is represented by three partially coupled linear equations. The development of models for actual materials would be an extremely difficult task.

LIST OF REFERENCES

LIST OF REFERENCES

1. Jenkin, C. F., "Fatigue in Metals," The Engineer, Vol. 134, Dec. 8, 1922, pp. 612-614.
2. Timoshenko, S. D., "Strength of Materials," Part 2, First edition, D. Van Nostrand Company, New York, 1930, pp. 679-680.
3. Iwan, W. D., "On a Class of Models for the Yielding Behavior of Continuous and Composite Systems," Journal of Applied Mechanics, Vol. 34, No. 3, Sept. 1967, pp. 612-617.
4. Drucker, D. C., "On the Continuum as an Assemblage of Homogenous Elements or States," Brown University Technical Report Number 50, 1966
5. Prager, W., "Models with Plastic Behavior," Proceedings of the 5th U.S. National Congress of Applied Mechanics, ASME, 1966 pp. 447-448.
6. Plummer, F. B., "Cyclic Plasticity and Structural Energy Dissipation," Ph.D. Thesis, University of Illinois, 1973
7. Whiteman, I. R., "A Mathematical Model Depicting the Stress-Strain Diagram and the Hysteresis Loop," Journal of Applied Mechanics, Vol. 26, 1959, pp. 95-100.
8. Caughey, T. K., "Sinusoidal Excitation of a System With Bilinear Hysteresis," Journal of Applied Mechanics, Vol. 27, 1960, pp. 640-643.
9. Thomson, W. T., "Analog Computer for Nonlinear System with Hysteresis," Journal of Applied Mechanics, Vol. 24, 1957, pp. 245-247.
10. Goodman, L. E., Klumpp, J. H., "Analysis of Slip Damping with Reference to Turbine Blade Vibration," Journal of Applied Mechanics, Vol. 23, 1956, pp. 421-429.
11. Iwan, W. D., "A Distributed Element Model for Hysteresis and its Steady State Dynamic Response," Journal of Applied Mechanics, Vol. 33, No. 4, pp. 893-900.
12. Bernard, J. E., "The Simulation of Coulomb Friction in Mechanical Systems," Simulation, Jan. 1980, pp. 11-16.

13. Meijers, P., Janssen, G. T. M., Booi, J., "Numerical Plasticity and Creep Analysis Based on the Fraction Model and Experimental Verification for WN 1.4948," Institute for Mechanical Constructions Publication, May 1975.
14. Bland, D. R., Lee, E. H., "On the Determination of a Viscoelastic Model for Stress Analysis of Plastics," Journal of Applied Mechanics, Vol. 23, 1956, pp. 416-420.
15. Martin, J. F., Topper, T. H., Sinclair, G. M., "Computer Based Simulation of Cyclic Stress-Strain Behavior with Applications to Fatigue" Materials Research and Standards, MTRSA, Vol. 11, No. 2, Feb. 1971, pp. 23-29.
16. Neuber, H., "Theory of Stress Concentration for Shear-Strained Prismatical Bodies with Arbitrary Nonlinear Stress-Strain Law," Journal of Applied Mechanics, Vol. 28, No. 4, Dec. 1961, pp. 544-560.
17. Bofferdig, C. H., "A Study of Cyclic Stress and Strain Concentration Factors at Notch Roots Throughout Fatigue Life," Master's Thesis, Michigan State University, 1980.
18. Lucas, L. J., "Experimental Verification of the Neuber Relation at Room and Elevated Temperatures," Master's Thesis, Michigan State University, 1982
19. Guillot, M. W., "An Experimental Evaluation of Neuber's Cyclic Relation at Room and Elevated Temperatures," Ph.D. Thesis, Louisiana State University, May 1981.
20. Leis, B. N., Topper T. H., "Cyclic Deformation and Fatigue Analysis for Notched Components," Nuclear Engineering and Design 20(1970), pp. 370-383.
21. Leis, B. N., Topper T. H., "Some Studies of the Influence of Localized and Gross Plasticity on the Monotonic and Cyclic Concentration Factors," Journal of Testing and Evaluation, JTEVA, Vol. 1, No. 4, July 1973, pp. 341-348.
22. Topper, T. H., Wetzel, R. M., Morrow, J., "Neuber's Rule Applied to Fatigue of Notched Specimens," Journal of Materials 4(1969), pp. 200-209.
23. Sharpe, W. N., Jr., "The Interferometric Strain Gage," Experimental Mechanics, Vol. 8, No. 4, April 1968, pp. 164-170.
24. Sharpe, W. N., Jr., "A Short Gage Length Optical Gage for Small Strain," Experimental Mechanics, Vol. 14, No. 9, 1974, pp. 373-377.
25. Meirovitch, L., "Analytical Methods in Vibrations," The Macmillan Company, New York, 1964, pp 56-61

26. Grantmacher, F. R., "The Theory of Matrices," Volume 2, Chelsea Publishing Company, New York, 1964, pp 113-114
27. Masing, G., "Eigenspannungen and Verfestigung Beim Messing," Proceedings of the Second International Conference on Applied Mechanics, Zurich, 1926, pp. 332-335.
28. Walker, K. P., "Research and Development Program for Nonlinear Structural Modeling with Advanced Time-Temperature Dependent Constitutive Relationships," NASA Report No. CR-165533, Nov. 1981.
29. Peterson, R. E., "Stress Concentration Factors," John Wiley and Sons, Inc., 1974, pp. 150-196.
30. Drucker, D. C., "A Definition of Stable Inelastic Material," Journal of Applied Mechanics, Vol. 26, 1959, pp. 101-106.
31. Slot, L., Stentz, R. H., Berling, J. T., "Controlled Strain Testing Procedures," Manual on Low Cycle Fatigue Testing, ASTM STP 465, American Society for Testing and Materials, 1969, pp. 100-128.
32. Hastelloy Alloy X Technical Data and Specifications, Cabot Corporation, Kokomo, Indiana, 1976.

MICHIGAN STATE UNIVERSITY LIBRARIES



3 1293 03177 5707